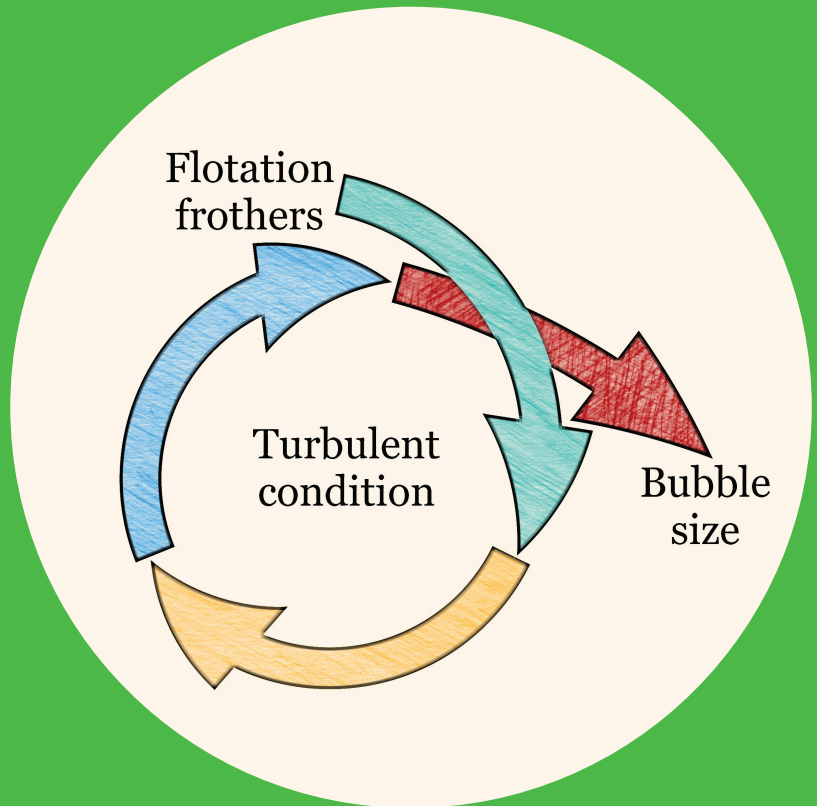


Frother controlled interfacial phenomena in dynamic systems - a holistic approach

Zoltán Jávör



Frother controlled interfacial phenomena in dynamic systems - a holistic approach

Zoltán Jávör

A doctoral dissertation completed for the degree of Doctor of Science (Technology) to be defended, with the permission of the Aalto University School of Chemical Technology, at a public examination held at the lecture hall V1 of the school on 26 November 2014 at 12.

Aalto University
School of Chemical Technology
Department of Materials Science and Engineering
Research Group for Mechanical Processing and Recycling

Supervising professor

Prof. Dr. Kari Heiskanen

Thesis advisor

Dr. Nóra Schreithofer

Preliminary examiners

Dr. Seher Ata, New South Wales University, Australia

Prof. Dr. Willy Kracht, University of Chile, Chile

Opponent

Prof. Dr. Cyril O'Connor, University of Cape Town, South Africa

Aalto University publication series

DOCTORAL DISSERTATIONS 161/2014

© Zoltán Jávör

ISBN 978-952-60-5911-2 (printed)

ISBN 978-952-60-5912-9 (pdf)

ISSN-L 1799-4934

ISSN 1799-4934 (printed)

ISSN 1799-4942 (pdf)

<http://urn.fi/URN:ISBN:978-952-60-5912-9>

Unigrafia Oy

Helsinki 2014

Finland



Author

Zoltán Jávör

Name of the doctoral dissertation

Frother controlled interfacial phenomena in dynamic systems - a holistic approach

Publisher School of Chemical Technology

Unit Department of Materials Science and Engineering

Series Aalto University publication series DOCTORAL DISSERTATIONS 161/2014

Field of research Mineral processing - Froth flotation

Manuscript submitted 5 June 2014

Date of the defence 26 November 2014

Permission to publish granted (date) 24 September 2014

Language English

Monograph

Article dissertation (summary + original articles)

Abstract

The development of froth flotation has revolutionized the mining industry and greatly increased the mineral production. Flotation reagents are widely applied to control the properties of minerals and bubbles in order to enhance the efficiency of froth flotation. Frothers are one of the flotation reagents employed to improve the performance of the process. The presence of frother molecules aids to reduce bubble size and rise velocity, and enhance froth stability. Although the effect of flotation frothers on bubble size is well known, the mechanism leading to the decrease in bubble size is not clearly understood.

In the present work, the effects of flotation frothers on bubble properties were examined in turbulent conditions. A new experimental framework was developed in order to understand the dynamic macro ($> 10^{-2}$ m)-, meso (10^{-5} to 10^{-2} m)- and micro/nano ($< 10^{-5}$ m)- scale phenomena affecting the bubble size in turbulent conditions. The new approach was aimed to explore the chain reaction triggered by the adsorption of surface-active agents, acting along the different size-scales and eventuating in decrease in bubble size.

To accomplish the aim, each and every size-scale was investigated in great detail and the results were correlated to each other. The micro/nano-scale phenomena affecting the bubble properties were investigated applying extensive dynamic surface property study such as dynamic surface tension, dynamic surface elasticity and adsorption/desorption rates. The meso-scale properties of bubbles (e.g. bubble rising velocity, bubble coalescence and breakup) were examined using newly designed experimental set-ups. The industrial or macro-scale properties of air bubbles were studied employing McGill Bubble Viewer. A series of common commercial frothers (DF200, NF240 and DF250) and two reagent grades (Pentanol and Polypropylene Glycol) were used during the study.

The main result of this work is a comprehensive, so far unavailable picture of the dynamics of surface-active molecules affecting bubble size in the presence of random momentum transfer. The adsorbed molecules diminish the tension at the air/liquid interface and increase its surface elasticity leading to a lower bubble rise velocity and modified coalescence and breakup properties that eventuate in smaller bubble size. The adsorption of weakly surface-active DF200 and Pentanol cause a different change in the properties of the air/liquid interface compared to the strongly surface-active DF250 and Polypropylene Glycol, leading to differences in size-scale properties and eventually in bubble size. The results help to understand the mechanism of flotation frothers and can provide information on possibilities to achieve better performance in mineral flotation by finding the most suitable surfactants for the particular process.

Keywords flotation frothers, turbulent condition, bubble size, dynamic surface properties

ISBN (printed) 978-952-60-5911-2

ISBN (pdf) 978-952-60-5912-9

ISSN-L 1799-4934

ISSN (printed) 1799-4934

ISSN (pdf) 1799-4942

Location of publisher Helsinki

Location of printing Helsinki

Year 2014

Pages 149

urn <http://urn.fi/URN:ISBN:978-952-60-5912-9>

Preface

This study was carried out at the Research Group for Mechanical Processing and Recycling at Aalto University, School of Chemical Technology during the years 2008-2014.

First, I wish to express my sincere gratitude to my supervisor Prof. Kari Heiskanen for giving me the opportunity to join his research group and for his excellent guidance during the thesis work. I am extremely grateful to Dr. Nóra Schreithofer for her endless encouragement and support during the years. Thank you for always finding time to advise me.

I want to thank all my present and former colleagues from the Research Group for Mechanical Processing and Recycling for the past years. Special thanks go to Ms. Iita Kejonen, Ms. Laura Tiainen, Mr. Toni Mattsson, Mr. Bosco Martinez and Mr. Ted Nuorivaara for their enormous amount of laboratory work. Thank you all!

I warmly thank Prof. Jim Finch for giving me the opportunity to spend valuable six months with his research team. I want to thank each and every members of the team for making my visit unforgettable. I particularly would like to thank Dr. Cesar O. Gomez, Dr. Wei Zhang, Dr. Miguel Maldonado, Dr. Jarrett Quinn, Mr. Patrick Blonde and Mr. Raymond Langlois for your advice, help and kindness.

I thank the preliminary examiners Dr. Seher Ata and Prof. Willy Kracht for providing valuable comments for improving the final draft of this work. I am very honoured to have Prof. Cyril O'Connor as my opponent.

The research work was founded by Academy of Finland and Finnish Metals and Engineering Competence Cluster (FIMECC). Their financial support is gratefully acknowledged.

Finally, I want to thank my family and friends for the endless support.

Espoo, 10 October 2014

Zoltán Jávör

Dedicated to my late grandma.

“For the want of a nail the shoe was lost,
For the want of a shoe the horse was lost,
For the want of a horse the rider was lost,
For the want of a rider the battle was lost,
For the want of a battle the kingdom was lost,
And all for the want of a horseshoe-nail.”

- Benjamin Franklin

List of publications

This thesis is based on the following publications, which are referred in the text by its Roman numerals.

- I. Jávora, Z., Schreithofer, N., Heiskanen, K. (2010) Fast adsorption phenomena at air/liquid interfaces. *XXV International Mineral Processing Congress*, Brisbane, Australia, pp. 2015-2023.
- II. Jávora, Z., Schreithofer, N., Heiskanen, K. (2012) The effect of bubble release techniques on their behaviour at the initial stages of rise. *Minerals Engineering*, **36-38**, 254-261.
<http://www.sciencedirect.com/science/article/pii/S0892687512001604>
- III. Jávora, Z., Schreithofer, N., Heiskanen, K. (2013) Validity of critical coalescence concentration in dynamic condition. *International Journal of Mineral Processing*, **127**, 16-22.
<http://www.sciencedirect.com/science/article/pii/S0301751613002354>
- IV. Jávora, Z., Schreithofer, N., Heiskanen, K., (2014) Micro- and nano-scale phenomena effect on bubble size in mechanical flotation cell. *Minerals Engineering (submitted)*
<http://www.sciencedirect.com/science/article/pii/S0892687514003136>
- V. Jávora, Z., Schreithofer, N., Gomez, C.O., Finch J.A., Heiskanen, K. (2014) Bubble breakup as a bubble size determining factor. *International Journal of Mineral Processing (submitted)*

Author's contribution

In **Publication I** and **II**, the author designed the experimental set-ups, planned and performed the experimental work, analysed the results, and wrote the manuscript under the supervision of the co-authors.

In **Publication III**, the author designed the experimental set-up and planned the experimental work performed by, or under the supervision of the author. The author, taking into account the comments of the co-authors, interpreted the results and wrote the manuscript.

In **Publication IV**, the author designed the experimental work performed under the direct supervision of the author and evaluated the data. The author, taking into account the comments of the co-authors, wrote the manuscript.

Publication V is a joint paper between McGill University and Aalto University. The experimental work was planned by the author and was performed by, or under the supervision of the author. The author, taking into account the comments of the co-authors, interpreted the data and wrote the manuscript.

Contents

LIST OF PUBLICATIONS	v
AUTHOR'S CONTRIBUTION	vi
CONTENTS	vii
LIST OF SYMBOLS AND ABBREVIATIONS	ix
1. INTRODUCTION	1
1.1 MACRO-SCALE	2
1.2 MESO-SCALE.....	3
1.3 MICRO/NANO-SCALE.....	3
1.4 SCOPE	4
1.5 OBJECTIVE.....	4
2. OVERVIEW OF PHENOMENA TAKING PLACE AT AIR/LIQUID INTERFACES	7
2.1 FLOTATION FROTHERS.....	7
2.2 ADSORPTION/DESORPTION PROPERTIES OF SURFACE-ACTIVE AGENTS.....	8
2.3 AIR/LIQUID INTERFACE PROPERTIES	10
2.4 BUBBLE PROPERTIES	11
2.4.1 <i>Rising velocity</i>	11
2.4.2 <i>Breakup</i>	12
2.5 BUBBLE-BUBBLE INTERACTION PROPERTIES.....	13
2.6 BUBBLE SIZE IN MECHANICAL FLOTATION CELL	14
2.6.1 <i>Sauter mean diameter</i>	14
3. EXPERIMENTAL	17
3.1 MATERIALS	17
3.2 METHODS AND APPARATUSES	18
3.2.1 <i>Study of adsorption/desorption properties</i>	18
3.2.2 <i>Study of air/liquid interface properties</i>	22
3.2.3 <i>Study of bubble properties</i>	23
3.2.4 <i>Study of bubble-bubble interaction properties</i>	28
3.2.5 <i>Study of bubble size in mechanical flotation cell</i>	29
4. EVALUATION OF THE MEASUREMENT DATA ACCURACY... 33	33
4.1 EVALUATION OF MICRO/NANO-SCALE DATA	33
4.2 EVALUATION OF MESO-SCALE DATA.....	35
4.2.1 <i>Accuracy of the bubble rising velocity study</i>	36
4.2.2 <i>Accuracy of the bubble breakup study</i>	37
4.2.3 <i>Accuracy of the bubble coalescence study</i>	39
4.3 EVALUATION OF MACRO-SCALE DATA	40
4.4 IMAGE PROCESSING AND CALIBRATION.....	41
5. MAIN RESULTS AND DISCUSSION	45
5.1 MICRO/NANO-SCALE RESULTS	45
5.2 MESO-SCALE RESULTS.....	49

5.2.1	<i>Bubble rising velocity</i>	49
5.2.2	<i>Bubble breakup</i>	50
5.2.3	<i>Bubble coalescence</i>	52
5.3	MACRO-SCALE RESULTS	54
5.4	INTERACTIONS BETWEEN SCALE DEPENDENT DYNAMIC PROPERTIES	56
6.	CONCLUSIONS	59
7.	RECOMMENDATIONS FOR FURTHER INVESTIGATIONS	65
8.	BIBLIOGRAPHY	67

List of Symbols and Abbreviations

Abbreviations

BPA	Bubble pressure analyser
BRVC	Bubble rise velocity column
DF	Dowfroth
fps	Frame per second
LBT	Langmuir-Blodgett trough
MBSA	McGill bubble size analyser
NF	Nasfroth
PD	Pulsation drop
PPG	Polypropylene Glycol
ppm	Parts per million
pw	Pure water with the resistivity of 15 M Ω
RPS	Alkaline detergent for ultrasonic cleaning
SBRC	Split bubble rise column
scm	Standard cubic centimetres per minute
SOC	Shear force observation chamber
upw	Ultra pure water with the resistivity of 18.2 M Ω

Symbols

A	Size reduction of the bubble [mm]
A _{Cell}	Sectional area of the flotation cell [m ²]
A _s	Surface area [cm ²]
b	Decay constant (LNo.05/CCC95)
C	Constant

List of Symbols and Abbreviations

c	Bulk concentration [ppm]
c _o	Equilibrium bulk concentration [mol/cm ³]
c(t)	Concentration in the sub-surface varies with time [mol/cm ³]
CCC	Critical coalescence concentration [ppm]
CCC ₉₅	Concentration giving 95% reduction in bubble size [ppm]
D	Diffusion coefficient [cm ² /s]
D ₃₂	Sauter mean diameter [mm]
D _b	Diameter of maximum stable bubble size [mm]
D _{eq}	Equivalent diameter [mm]
D _h	Horizontal diameter of air bubble [mm]
D _L	Limiting or minimum bubble size [mm]
D _{rot}	Diameter of rotor [m]
D _{SV}	Surface volume diameter [mm]
D _V	Vertical diameter of the bubble [mm]
E	Surface dilational modulus
E'	Pure surface elasticity or storage modulus
E''	Surface viscosity or loss modulus
E _{eff}	Effective or dynamic surface elasticity [mN/m]
E _G	Gibbs or static surface elasticity [mN/m]
F	Force on the Wilhelmy plate [mN]
g	Gravitational constant, [N(m/kg) ²]
i	imaginary unit ($\sqrt{-1}$)
J _g	Superficial gas velocity [cm/s]
L	Immersed perimeter of Wilhelmy plate [mm]
N	Revolution per minute of the rotor
P/V	Power input per unit of volume
Q _g	Volumetric flow rate of air [m ³ /s]
R	Radius of forming bubbles [mm]
R _o	Radius of the bubble curvature at apex [mm]
r	Radius of capillary [mm]
S	Surface area [mm ²]

S_b	Bubble surface area flux [s^{-1}]
S_{rot}	Rotor tip speed [m/s]
S_V	Volume-specific surface [mm^2/mm^3]
T_b	Bubble lifetime [sec]
U_T	Terminal velocity of particle [cm/s]
V	Volume [mm^3]
ν	Pulsation frequency [Hz]
We	Weber number

Greek Symbols

β	Shape factor
Γ	Interfacial concentration of surface (or surface excess) [mol/cm^2]
Γ_o	Equilibrium interfacial concentration of surface [mol/cm^2]
γ	Surface tension [mN/m]
γ_o	Initial tension of the surface [mN/m]
γ_d	Dynamic surface tension [mN/m]
γ_{dl}	Long-term dynamic surface tension (up to 20 min) [mN/m]
γ_{ds}	Short-term dynamic surface tension (up to 10 sec) [mN/m]
η	Surface dilatational viscosity
Π	Surface pressure [mN/m]
θ	Contact angle between the Wilhelmy plate and the liquid [$^\circ$]
ρ	Density of the continuous phase [g/cm^3]
$\Delta\rho$	Density difference via air/liquid interface [g/cm^3]
ρ_l	Density of the liquid [g/cm^3]
τ	Thickness of the interface [cm]

1. Introduction

Most of the mined minerals are not suitable for direct use as a final product without further preparation and separation processes. Froth flotation is a widely applied dynamic physico-chemical separation process where surface-active agents establish the optimal setting for separating valuable minerals from unwanted gangue. Air bubbles are employed to accomplish the separation. In mechanical flotation cells, the bubbles are formed from gas dispersed into the pulp phase via an impeller. Rotation of the impeller creates dynamic conditions in the pulp phase essential to disperse the air, to keep particles in suspension and to facilitate bubble-particle interactions. Bubbles formed under dynamic conditions rise in the pulp phase and form a froth bed on the top of it. During the rise, the bubbles first pass through a turbulent zone and then a quiescent zone.

Flotation frothers are commonly employed to aid air dispersion. Frothers are surface-active agents with the primary aim to reduce the size and the rising velocity of the bubbles, and to enhance froth stability (Harris, 1976; Rao, 2004; Zhang et al., 2012). The focus of the present work is to gain deeper understanding on the effect of frothers on bubble size and bubble rising velocity; nevertheless, the study of the froth phase was out of the scope of this thesis.

Sauter mean diameter (D_{32}) is an industrial index widely employed to characterise frother effect on bubble size in flotation cells. The bubble samples used for calculating D_{32} are collected from the quiescent zone of the cell. The quiescent zone makes available to monitor bubbles size with low sensitivity to the position of the sampling tube, consequently the measurement is easily reproducible. These results perfectly characterise the size of the bubbles building up the froth phase. The position of the sampling tube is much more crucial when bubbles are collected from the turbulent zone where the actual particle-bubble interaction takes place in three-phase systems. The size of bubbles passing through the turbulent zone, colliding with particles and executing the particle transport from the pulp can differ from that building up the froth phase.

When the magnitude of viscous forces on the fluid is higher compared with other forces, the disturbances introduced into the system will tend to be damped out leading to a quiescent or laminar flow. On the other hand, when the inertial forces rise, the fluid will break up into eddies creating turbulent flow (Richardson, 1922). The higher the turbulent kinetic energy, the more eddy breakup occurs leading to smaller eddies (energy cascade). This will continue until the smallest size scale is reached where the viscous forces dominate again (Kolmogorov, 1941). The turbulent flow field can be described by the Navier-Stokes equation in case the turbulence is considered as a continuum phenomenon (significantly large length scale). Nevertheless, describing the flow field in practice is much more complex due to random phenomena. Statistical analyses are widely applied tools used to simplify the complexity of turbulent flows. The statistical approach suits engineering design purposes; however, using statistical analyses in order to gain understanding of bubble properties in turbulent flow could be misleading.

The surface coverage of a bubble moving through a quiescent zone is in quasi-equilibrium; therefore, the surfactant concentration remains constant at any surface unit area in a sense of Eulerian frame of reference. This approximation will not be true if the bubble moves through a turbulent zone. Local random momentum transfer will arise due to the Kolmogorov eddy cascade leading to bubble oscillation and wobbling. The surface oscillation disturbs the local equilibrium and causes temporal surface excess. These phenomena in turn cause surface stresses counteracting the deformation (Miller and Liggieri, 2009). This is called dynamic conditions in this work, while the quasi-equilibrium is called static condition.

Since there is no exact solution to investigate the governing phenomenon affecting bubble size in turbulent conditions, only in simplified equilibrium cases, many relationships can be derived based on size-scale analyses. According to Wierink (2012) the frother effect on bubble size in dynamic condition can be investigated in three size-scales (Figure 1.1):

Macro-scale to industrial scale (characteristic length $> 10^{-2}$ m);

Meso-scale (characteristic length 10^{-5} to 10^{-2} m);

Micro/nano-scale to molecular scale (characteristic length $< 10^{-5}$ m).

1.1 Macro-scale

Gas dispersion parameters are employed to quantify the macro-scale properties of air bubbles dispersed into the mechanical flotation cell. The Sauter mean diameter (D_{32}) is considered a relevant gas dispersion parameter in the flotation process (Gorain et al., 1995). The D_{32} determines the bubble surface area flux (S_b) that is the available surface area for transporting

particles during the flotation process and thereby influences the process efficiency (Xu et al., 1991; Finch et al., 1999).

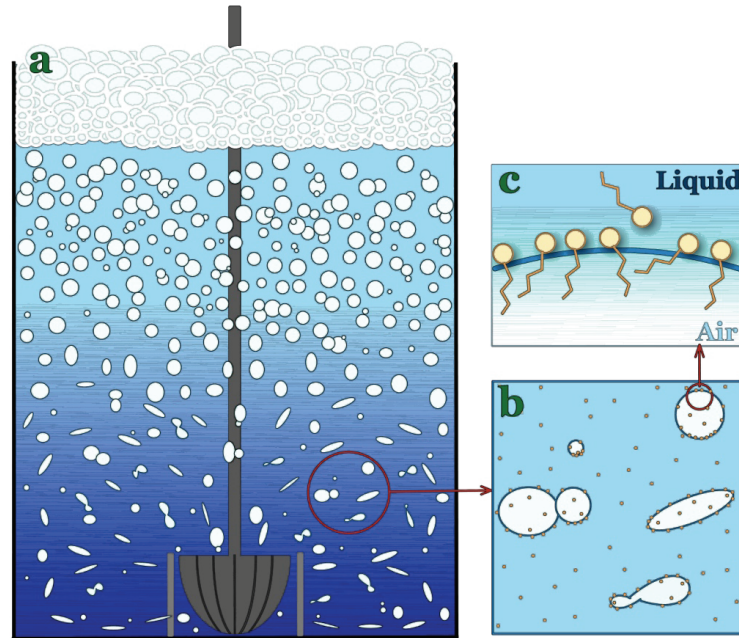


Figure 1.1 Scale-dependent phenomena in flotation a) macro-scale; b) meso-scale; c) micro/nano-scale.

1.2 Meso-scale

The bubble size observed in mechanical flotation cells (D_{32}) is determined by bubble coalescence and breakup (Gorain et al., 1995; Grau and Laskowski, 2006). The decrease in bubble size reduces the rising velocity of the bubbles and increases the gas holdup (Sam, 1995). Different frothers may lead to the same gas holdup but the bubble swarm composition could be different suggesting that the frother affects the rising velocity of the swarm (Azgomi et al., 2007; Kracht and Finch, 2010).

1.3 Micro/nano-scale

Bubble breakup is caused by hydrodynamic stresses of size and magnitude that are capable of disrupting the bubble surface (Hinze, 1955). In the presence of frothers, the resistivity of bubbles against hydrodynamic stresses depends on the dynamic elasticity property of the air/liquid interface (Walter and Blanch, 1986). During bubble breakup, a significant surface deformation leads to the deviation of surface tension compared with the equilibrium. The

magnitude of the deviation depends on the adsorption properties of the frothers that tend to restore the equilibrium (Janssen et al., 1994).

Colliding bubbles coalesce when the interfacial liquid film becomes thinner and ruptures. The dynamic elasticity of the air-liquid interface is a factor determining the drainage rate and indicates that the less mobile the surface, the slower the drainage (Marrucci, 1969).

1.4 Scope

As expressed by Nasset et al. (2012), the bubbles unquestionably constitute the heart of the flotation process. The size and the surface area of the bubbles substantially determine the recovery of the flotation process (Pogorely, 1962; King, 1972). The importance of bubble properties during the flotation process was recognised already in 1916 by Rickard; however, due to the lack of proper technical facilities, these studies were deferred till the early 21st century.

In the past 20 years, a wide range of new findings has been introduced about the effect of frothers on the air/liquid interface approached on different size-scales. (e.g.: Sam, 1995; Sweet et al., 1997; Beverung et al., 1999; Millet et al., 1999; Krzan and Malysa, 2002; Cho and Laskowski, 2002a, b; Grau and Heiskanen, 2002; Hernandez-Aguilar et al., 2002, Nasset et al., 2007; Nasset et al., 2012; Maldonado et al., 2013). However, the interactions between the different size-scales phenomena have not been explored.

Most of the existing studies investigate the frother effect in quiescent conditions leading to new, interesting and essential knowledge. Nevertheless, understanding of frother effect in turbulent conditions would be crucial for the comprehension of industrial systems.

In the present work, the effects of flotation frothers on the properties of air bubbles are presented. For the first time, a full-scale analysis was accomplished with the primary aim to identify the relationship between the size-scale determined surface properties leading to the decrease in bubble size. In addition, the equilibrium was disrupted during each size-scale property study; therefore the effect of turbulent conditions on the surface properties was explored in detail. Each result presented in this work is the achievement of a comprehensive, in depth investigation.

1.5 Objective

The present study aims at understanding the frother effect on bubble properties in turbulent conditions applying a new size-scale determined experimental approach. The new technique was developed in order to systematically explore the chain reaction triggered by the adsorption of surface-active agents and acting along different size-scales. The adsorption of

flotation frothers affects the properties of air/liquid interface leading to a change in bubble properties and bubbles interaction properties that eventuate in smaller bubble size. The framework of the new experimental approach is presented in Figure 1.2.

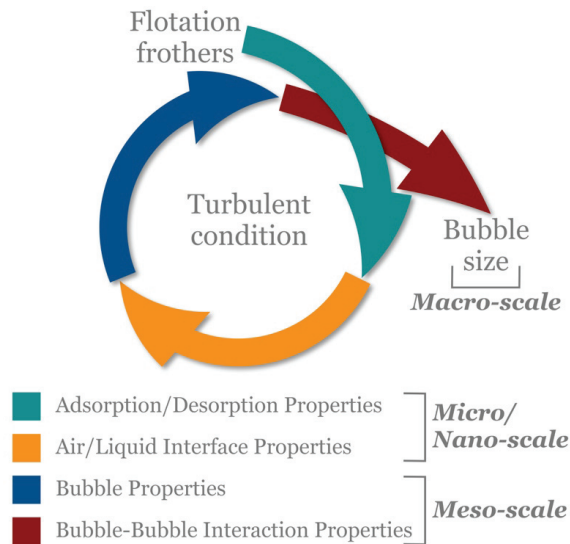
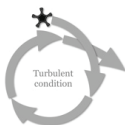


Figure 1.2. Representation of the experimental framework highlighting the relationship between the size-scale determined surface properties leading to the decrease in bubble size.

A new experimental approach was required for studying the frother effect with a wide variety of measurement techniques in all the three size-scales, but special attention was paid to the undiscovered dynamic meso-scale properties. Laboratory equipment can be employed to study the micro/nano-scale properties while industrial bubble size analysers allow monitoring of macro-scale properties; however, there are no existing method for studying dynamic meso-scale properties. Therefore, newly designed experimental set-ups were required allowing to simulate dynamic properties corresponding to the one in mechanical flotation cells, in order to discover the dynamic meso-scale properties.

2. Overview of phenomena taking place at air/liquid interfaces

It is well established that the presence of surface-active agents diminishes the size of the bubbles dispersed into mechanical flotation cells. The decrease of bubble size aids the efficiency of flotation process. In order to be able to optimise the process it is crucial to understand the phenomena taking place at the air/liquid interfaces in great depth. The adsorption of the surface-active agent triggers a chain reaction acting along different size-scales and leading to the decrease of bubble size. In the present chapter, this chain reaction is followed through the micro/nano (10-10 to 10-5 m)-, meso (10-5 to 10-2 m)- and macro (> 10-2 m) scales.



2.1 Flotation Frothers

Flotation frothers are heteropolar surface-active agents applied in industrial flotation process to stabilize bubble surface and form froth bed on the top of the pulp. Frother molecules are composed of a hydrophilic head and a hydrophobic tail. The hydrophilic head is polar group such as hydroxyl (OH), carboxyl (COOH), carbonyl (C=O) and ester (COOR) (Wrobel et al., 1953, Laskowski, 1998), while the hydrophobic tail is a hydrocarbon chain classified based on chain length and structure. During the adsorption process, the head orients towards the water and the tail towards the air making the composition and structure of the head and tail crucial on adsorption properties (Figure 2.1).

Commercially there are two main frother classes (Zhang, 2009): alcohols and polyglycols. From the industrial point of view, alcohols are “weak frothers” due to their tendency to produce a relatively shallow froth (Cyttec, 2002). From the point of view of surface chemistry, the alcohols are weakly surface-active agents and therefore unable to decrease the surface tension appreciably (Laskowski 1998). The MIBC and pentanol are commonly employed alcohols in industrial flotation processes. Polyglycols are highly surface-active agents with the ability to diminish surface tension appreciably and create deep froth. Dowfroths (DF) and Polypropylene Glycol (PPG) are widely applied polyglycols in industrial flotation processes.

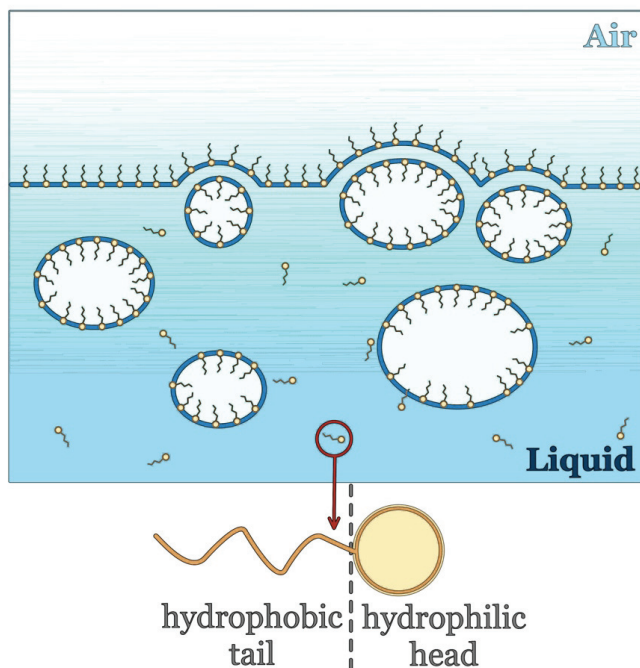


Figure 2.1. Common structure of flotation frother and its bubble stabilizing action

2.2 Adsorption/desorption properties of surface-active agents



The exchange of molecules between the bulk solution and the air/liquid interface is a dynamic surface activity, determined by the adsorption and desorption properties of the molecules.

According to Derjaguin and Dukhin (1961), the air/liquid interface can be divided into three layers (Figure 2.2): the actual interface, the sublayer and the bulk solution. Bulk solution is considered to be a liquid with uniform concentration of surface-active agents. During the time scale, a three-step adsorption process takes place (van den Tempel and Lucassen-Reynders, 1983):

- *diffusion* of surfactant to the sub-layer from the bulk solution;
- *actual adsorption* from the sub-layer to the surface, retreating is possible due to an adsorption barrier;
- *re-arrangement* such as reorientation, complex formation, chemical reactions and phase transitions of adsorbed surfactant.

The surface coverage (Γ) of the air/liquid interface increases with time as more and more molecules adsorb leading to decrease of surface tension. Molecule adsorption takes place on the interface until the equilibrium coverage (Γ_0) is reached (Figure 2.2). A non-equilibrium state of the surface

can result from the absence of sufficient adsorption time required to reach the equilibrium surface coverage at a freshly formed interface or the distortion of the surface with equilibrium coverage (Malysa and Lunkenheimer, 2008). When the equilibrium surface coverage is disturbed the coverage could either be below the equilibrium ($\Gamma < \Gamma_0$) leading to further adsorption or above it ($\Gamma > \Gamma_0$) giving rise to molecules desorption.

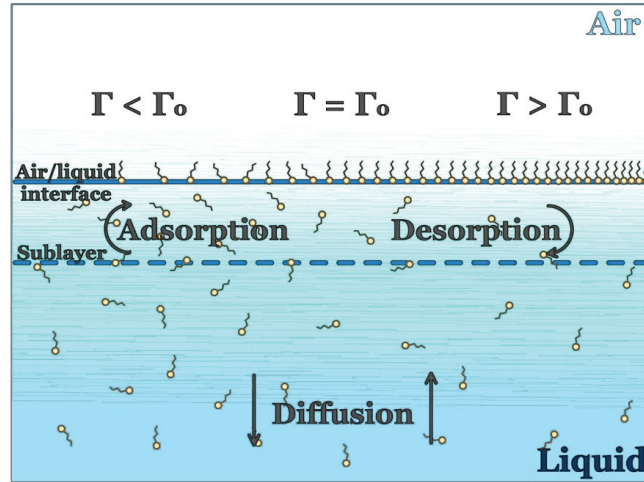
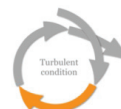


Figure 2.2. Molecules exchange at the air/liquid interface (based on: Dukhin et al., 1995)

The first time-dependent adsorption model was introduced by Ward and Tordai (1946). This kinetic model approaches the change of interfacial tension as a result of surface coverage caused only by diffusion in the absence of any liquid flow. The model is called diffusion-controlled adsorption kinetics model:

$$\Gamma(t) = 2 \sqrt{\frac{D}{\pi}} \left(c_0 \sqrt{t} - \int_0^{\sqrt{t}} c(0, t - \tau) d\sqrt{\tau} \right) \quad (\text{Eq. 2.1})$$

where D is the diffusion coefficient, τ is the thickness of the interface and c_0 is the surface bulk concentration. The diffusion-controlled model and the kinetic-controlled model are the two general approaches describing the dynamics of adsorption at air/liquid interfaces (Dukhin et al., 1995). The diffusion-controlled model regards the diffusional transport of the molecules from the bulk to the interface as a determining factor of the adsorption rate (Milner, 1907) while the kinetic model regards the transfer mechanisms of the molecules from the sublayer to the interface as the rate-controlling process (Doss, 1939; Ross, 1945).



2.3 Air/liquid interface properties

The adsorbed surfactants decrease the surface tension and stabilize the air/liquid interface. Nevertheless, the properties of the air/liquid interface are substantially determined by the rheological properties of the adsorbed layers (Fruhner et al., 1999). When the equilibrium of the interface is disturbed, a spontaneous process arises to restore equilibrium in the system. The equilibrium can be restored by the re-arrangement of molecules leading to elastic surface property; hence the film rupture is less likely to occur.

Gibbs (1931) was the first who defined surface elasticity (E_G) as a variable resistance to surface deformation (Eq. 2.2). The Gibbs elasticity proposes an isothermal equilibrium condition where the change of surface area causes changes in surface coverage and consequently in surface tension. Nevertheless, the restoration of equilibrium surface coverage is not taken into consideration.

$$E_G = \frac{2 \cdot d\gamma}{d \ln A_s} \quad (\text{Eq. 2.2})$$

Under dynamic conditions, the adsorbed molecules provide a restoring force and therefore protect the film from local thinning (Figure 2.3a). The phenomenon is called Marangoni effect and it is triggered by the tension gradient of the surface. However, the restoring force only arises when the concentration of the surfactant is ideal in the solution as it was highlighted by Harris (1976). In high frother concentrations, the molecule diffusion from the bulk could occur before the restoring, subsequently forming a thinned segment and making the air/liquid interface more willing to rupture (Figure 2.3b).

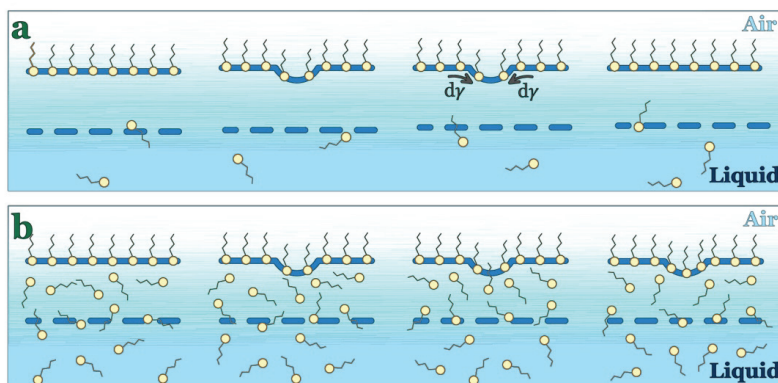


Figure 2.3. Concentration effect of frothers on dynamic surface properties (based on: Harris 1982)

In the presence of turbulent eddies, the equilibrium surface coverage is never reached at the disturbed air/liquid interface. Therefore, the surface elasticity,

arises against hydrodynamic stresses and should be derived from non-equilibrium surface state. The surface elasticity observed in non-equilibrium condition is called effective or dynamic elasticity (E_{eff}), a concept introduced by Malysa (1992).

Two experimentally measurable parameters are employed to determine rheological properties of surface, e.g. pure surface elasticity (E') and surface viscosity (E''). Pure surface elasticity is the extent of the stored energy in the surface layer as a result of external stress, while surface viscosity is the measure of the dissipation energy.



2.4 Bubble properties

The frother effect on surface mobility has also been detected during bubble rise velocity (Clif et al., 1978; Krzan and Malysa, 2002) and also bubble breakup studies (Walter and Blanch 1986).

2.4.1 Rising velocity

The terminal velocity of a rigid sphere moving through a continuous medium is lower than that of an air bubble of the same size and density. The difference in terminal velocity arises due to the internal circulation inside the air bubble (Hadamard, 1911; Rybczynski, 1911).

On the surface of an air bubble moving through a liquid solution, the adsorbed molecules are swept from the frontal region to the rear part of the bubble due to the surface advection caused by the main flow around the bubble. The concentration of the molecules increases at the rear of the bubble as a result of the surface flow producing a surface tension gradient. This surface tension gradient generates a viscous shear stress (Marangoni effect) modifying the surface flow and increases the drag, consequently decreasing the bubble rise velocity (Frumkin and Levich, 1947; Levich, 1962).

The molecule re-arrangement on the surface of air bubbles affects the internal circulation and it is pushed forward to the frontal region leaving a stagnant rear region. Savic (1953) was the first to calculate the terminal velocity by measuring the angles of the stagnant rear region (stagnant cap). The stagnant cap forms when the adsorption and desorption kinetic is slow compared to the surface convection (Cuenot et al., 1997).

The local velocity of a bubble changes as a function of the distance travelled from the release point of the orifice until a constant terminal velocity is reached (Ayberts and Tapucu, 1969). Sam (1995) observed three distinct stages in the change of local velocity as a function of distance (Figure 2.4). In the first stage, the bubble accelerates quickly (≈ 0.2 sec) from the initial stationary state to its maximum velocity. In the second stage, the bubble

decelerates due to the increase of the drag force caused by a change in the bubble surface properties. The frother type and concentration affect the rate of deceleration. In the final stage, terminal velocity is reached when the drag force becomes equal to the buoyancy force. Bubble size and frother type determine the terminal velocity.

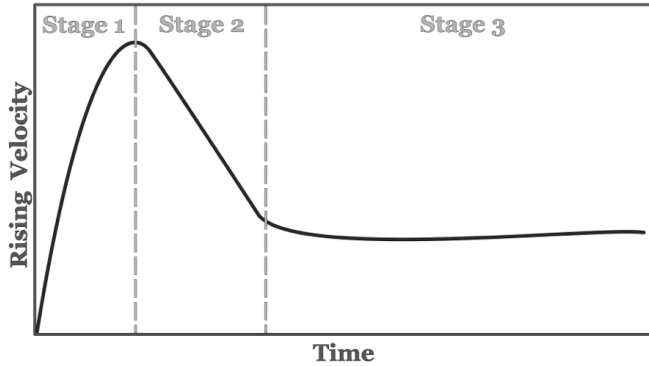


Figure 2.4. Stages of bubble rising velocity profile (based on: Sam, 1995)

The latest study of Maldonado et al., (2013) points out a unique relationship between bubble shape and rising velocity (ca. 1.2 m above the release point), independent of solute type and concentration.

2.4.2 Breakup

Bubble breakup is caused by hydrodynamic stresses of size and magnitude that are capable of disrupting the bubble (Hinze, 1955). Bubble breakup depends on the balance of disruptive and cohesive force effect on the bubble in dynamic conditions. The dimensionless Weber number is a widely applied term to express this balance:

$$We = \frac{U_T^2 D_b \rho_l}{\gamma} \quad (\text{Eq. 2.3})$$

The critical Weber number (We) introduced by Calderbank (1958) applied to estimate the maximum stable bubble size where the disruptive and cohesive forces balance. Walter and Blanch (1986) proposed that the maximum stable bubble size could be estimated from,

$$D_b = C \frac{(\gamma + E)^{3/5}}{\left(\frac{P}{V}\right)^{2/5} \rho^{1/5}} \quad (\text{Eq. 2.4})$$

In the presence of frother, the resistivity of bubbles against hydrodynamic stresses depends on the surface elasticity that become higher with longer frother chain length (Walter and Balanch, 1986).

During the froth flotation process, turbulent flow conditions are applied in order to maximize the interfacial area of the dispersed air (Clift et al., 1978). The shear stress induced by the continuous phase deforms the bubbles and breaks them when it overcomes the counterbalancing effect of surface tension force. Shear stress is only caused by eddies with the size smaller than the bubbles while the larger eddies only transport them (Hinze, 1955).

In mechanical flotation cells, gas cavity is formed in the first step at bubble generation at the low pressure tailing edge of the impeller (Rennie and Valentin, 1968) and from the tail of the cavity, bubbles are shed by turbulent eddies (Grainger-Allen, 1970) indicating bubble breakup mechanism. Two different bubble formation processes are observed from cavity (Grainger-Allen, 1970; Michel, 1984; Rigby et al., 1997): surface instability caused large bubble “pinch off” from the top of the interface and cascading wave caused small bubble formation on the lower interface (Figure 2.5).

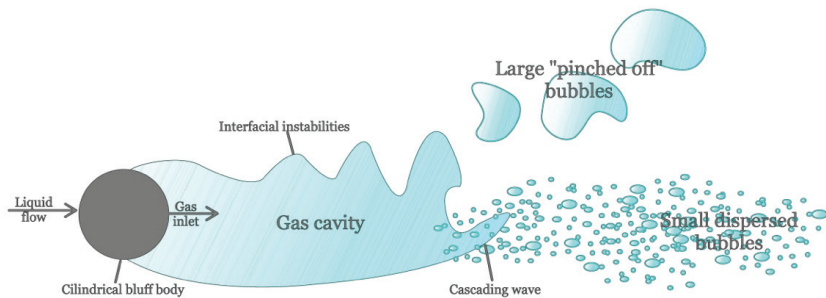
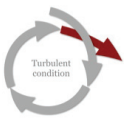


Figure 2.5. Schematic of bubble breakup from cavity (based on: Rigby et al., 1997)

Bubble breakup could also result from bubble coalescence (Machon et al., 1997; Tse et al., 2003; Quinn and Finch, 2012). The phenomenon was named coalescence-induced breakup and it is explained by the action of annular wave followed after film rupture.



2.5 Bubble-bubble interaction properties

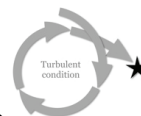
External forces direct bubbles moving through a continuous medium to approach each other and collide (Chaudhari and Hoffmann, 1994). There is trapped liquid between the colliding bubbles that drains with time. When the contact time is sufficient the drainage of trapped liquid (film) leads to a critical film thickness (Marrucci, 1969; Chesters, 1991). If the critical film thickness is reached, the film ruptures and coalescence occurs. However, if the contact time is less than the film drainage time, they will separate again without coalescing (Machon et al., 1997).

The coalescence itself occurs within three steps (Oolman and Blanch, 1986):

1. Surfaces of the two colliding bubbles are flattened and only separated by a thin liquid film (typically $10 - 10^0 \mu\text{m}$ thick) upon the impact point;
2. The film between the two bubbles becomes thinner ($\approx 10^{-2} \mu\text{m}$) due to the drainage of the liquid;
3. Instability of the thin film causes rupture on the interface and formation of a coalesced bubble.

The contact time required for coalescence becomes longer with increasing frother concentration (Sagert et al., 1976). Clean air/liquid interface (absence of flotation frothers) cannot support a shear stress; therefore, there is a slip boundary condition during drainage. Nevertheless, the presence of flotation frothers at the interface can change the boundary condition to partial-slip or non-slip leading to slower drainage speed (Henry et al. 2007). The drainage speed is not only determined by frother type and concentration but the approach speed of the bubbles (Kirkpatrick and Lockett, 1974; Yaminsky et al. 2010, Castillo et al. 2011). Even in purified water the coalescence time of bubbles can be extended from milliseconds to minutes when the approach speed of the bubbles is sufficiently low (Castillo et al. 2011). The film thinning is conducted by such local hydrodynamic properties of the interface as surface elasticity and surface tension gradient.

2.6 Bubble size in mechanical flotation cell



Froth flotation is a separation process where dispersed air is employed to transport the desired particles from the pulp to the froth, therefore the efficiency of the flotation process is determined by the surface area of bubbles accessible to particles (Pogorely, 1962; King, 1972). The measurement of bubble behaviour in the industrial environment became possible with the advent of industrial sensors developed by McGill University (Gomez & Finch, 2002) and by JKMR (Schwarz & Alexander, 2006). The measured data facilitates the definition of the key process parameters by mathematical expressions (Nesset et al., 2012).

2.6.1 Sauter mean diameter

There are two essential particle properties: surface (S) and volume (V) (Allen, 1990). The ratio of surface to volume determines the volume-specific surface (S_V):

$$S_V = \frac{S}{V} = \frac{\pi D_S^2}{\frac{\pi}{6} d D_V^3} = \frac{6}{D_{SV}} \quad (\text{Eq. 2.5})$$

where D_{SV} is the surface volume diameter, which express the diameter of a sphere possessing the same external surface to volume ratio as a particle of interest. Finch and Dobby (1990) determined the bubble surface area flux (S_b)

based on Eq. 2.5. The bubble surface area flux defines the surface area of the bubbles existing in the unit cross-section of the flotation cell per unit of time (Xu et al., 1991; Finch et al., 1999):

$$S_b = \frac{6J_g}{D_{32}} \quad (\text{Eq. 2.6})$$

where J_g is the superficial gas velocity and D_{32} is the Sauter mean diameter of the bubble. Superficial gas velocity is the volumetric flow rate of the introduced air (Q_g) per unit cross the sectional area of the cell (A_{cell}):

$$J_g = \frac{Q_g}{A_{cell}} \quad (\text{Eq. 2.7})$$

Sauter mean diameter is a surface, volume mean diameter representing the whole bubble population. The purpose of mean diameter is to represent a group of individual value in order to understand the group (Figure 2.6) (Allen, 1990). The D_{32} is derived from the measured equivalent diameter (D_{eq}) by Hernandez-Aguilar et al., (2005):

$$D_{32} = \frac{\sum dV}{\sum dS} = \frac{\sum D_{eq}^3}{\sum D_{eq}^2} \quad (\text{Eq. 2.8})$$

The parameter representing the volumetric fraction of gas in the cell is called gas holdup (E_g). This parameter along with the S_b , J_g and D_{32} become known as the gas dispersion parameters. Gas dispersion parameters are measured in industry in order to optimise the efficiency of the flotation process.

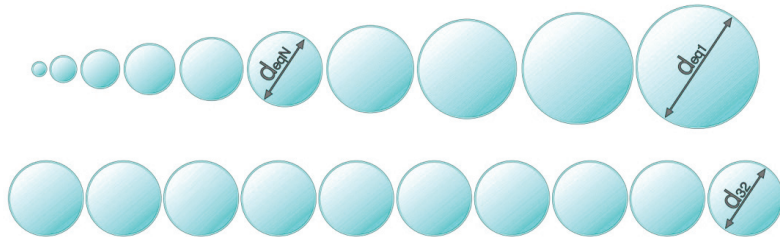
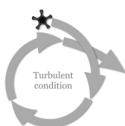


Figure 2.6. The homogeneous distribution representing the heterogeneous distribution of ten particles (based on Allen, 1990)

3. Experimental

The wide variety of measurement methods and techniques employed to study the frother effect on the properties of the air/liquid interface are described in more detail in Chapter 3.2. The materials used in the work are introduced in Chapter 3.1.



3.1 Materials

The experimental work focused on studying the effect of surface-active agents on bubble properties. Five individual frothers (Table 3.1) were systematically investigated. Two reagent grades, the 1-Pentanol and the Polypropylene glycol 425 (PPG425 that industrial name is F150), with $\approx 99\%$ purity were distributed by Aldrich-Sigma. The two chemicals were chosen due to their different chemical structure. The 1-Pentanol is a weakly surface-active alcohol while the PPG425 is highly surface-active polyglycol. Three commercial polyglycol frothers were also studied, the Dowfroth 200 (DF200), Nasfroth 240 (NF240) and the Dowfroth 250 (DF250) distributed by Nasaco International Ltd.

Table 3.1. List of frothers used in the experiments

Name of frothers	Short name of frothers	Chemical formula	Molecular weight [g/mol]
1-Pentanol	1-Pentanol	$C_5H_{12}O$	88.15
Dowfroth 200	DF200	$CH_3(OC_3H_6)_3OH$	206.28
Nasfroth 240	NF240	$C_4H_9(OC_2H_4)_3OH$	206.28
Dowfroth 250	DF250	$CH_3(OC_3H_6)_4OH$	264.37
Polypropylene glycol	PPG425	$H(OC_3H_6)_7OH$	≈ 425

Sample solutions for micro/nano-scale measurements were prepared from ultra pure water (upw), with 18.2 M Ω resistivity produced with *Millipore Direct-Q* water purification system. The upw was purified in four steps

including pre-treatment, reverse osmosis, ion exchange and UV treatment. The high water purity and steady medium quality is crucial during molecular scale studies in order to undoubtedly identify the frother effect on air/liquid interface properties in micro/nano-scale. Meso-scale measurements required a bigger volume of sample solution therefore a high capacity *Elga Purelab Option R 15 BP* water purification system was used to produce pure water (pw) with the resistivity of 15 M Ω . The pw is also purified in four steps including pre-treatment, reverse osmosis, UV treatment and ion exchange. The water volume required for macro-scale measurements was very large to be produced even with the high capacity water purification system therefore Espoo (Finland) tap water with the resistivity of 0.014 M Ω was used during the two-phase, mini-pilot flotation tests.

The typical tap water conductivity ranges from 50 to 800 η S/cm (State Water Board, 2002) and the conductivity of Espoo tap water is in the lower end of the range (71.3 η S/cm) suggesting high water purity. Therefore, the impurity of Espoo tap water should not have an effect neither on the micro/nano-scale, the meso-scale nor the macro-scale measurements. Nevertheless, using upw for the micro/nano-scale measurements and pw for meso-scale measurements allows reproducing the experiments in different locations without affecting the results. Another benefit of purified water is the steady water quality, unlike the tap water, which provides variable water quality caused by certain conditions (e.g. after holidays when water is stored in the pipeline for a longer time, after pipe breakage, after heavy rains, etc.).

3.2 Methods and apparatuses

3.2.1 Study of adsorption/desorption properties

The surface tension (γ) and surface pressure (Π) measurements are widely applied methods to characterise the surface activity and the adsorption/desorption properties of surface-active substances including flotation frothers. Both of these methods were employed during the present work in order to acquire a deeper knowledge of the adsorption/desorption properties of flotation frothers.

Surface tension measurement

Surface tension arises as the result of the attractive force acting in every direction equivalently between molecules of the medium. On the surface of the medium these intermolecular forces are unbalanced due to the excess free energy. The surface tension of the air/liquid interface formed in ultra pure medium (upw) is 72.8 mN/m at room temperature. In the presence of surface-



active agents the surface tension decreases, due to the molecule adsorption, until the equilibrium surface coverage is reached (Figure 3.1).

Equilibrium surface coverage occurs when the adsorption/desorption rates are in equilibrium and therefore a static surface tension is achieved. The surface tension measured during the adsorption process is called dynamic surface tension (γ_d).

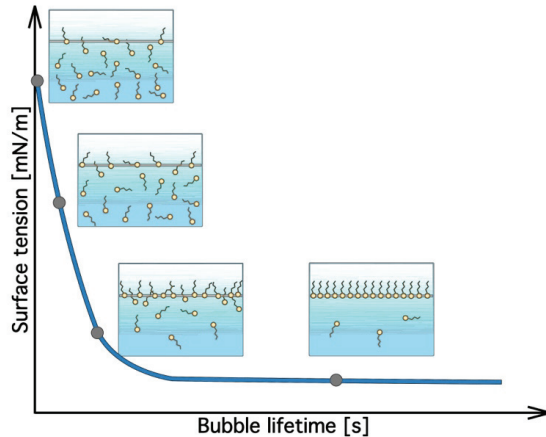


Figure 3.1. Frother effect on surface tension as a function of bubble lifetime (based on: Biolin Scientific, Attension Theory Note 2)

Bubble Tensiometry (BPA-800P)

The BPA-800P (produced by Attension; formerly KSV Instruments) applies the maximum bubble pressure method to measure the dynamic surface tension of the air/liquid interface. Mysels (1990) reviewed the method extensively. Dynamic surface tension is calculated from the pressure of the bubble formed at the tip of capillary. The capillary immersed into the test solution generates bubbles with steady airflow rate and the fluctuation in pressure is monitored inside the capillary (Figure 3.2). From the initial stage of bubble formation the pressure increases moderately until its maximum is reached. The maximum bubble pressure is observed when the radius of the forming bubbles (R) becomes identical with the radius of the capillary (r). After the maximum bubble pressure is reached the pressure drops rapidly.

The time interval, from bubble formation until the maximum bubble pressure is reached, is called bubble lifetime. During the study the frequency of bubble generation decreases, concurrently the lifetime of the bubble increases and the time dependency of surface pressure on air/water interface is determined. The method enables measuring the bubble lifetime within a short-term (up to seconds).

The BPA-800P calculates the short-term dynamic surface tension (γ_{ds}) from the measured pressure difference between the initial system pressure (P_s) and

the maximum hydrostatic pressure ($P_{h,max}$) of the liquid at the capillary tip based on the Laplace equation (Fainerman et al. 1998):

$$\gamma_{ds} = \frac{r \cdot \Delta P}{2} \quad (\text{Eq. 3.1})$$

The dynamic surface tension results measured with the BPA-800P are reported in **Publication I, II, IV and V**.

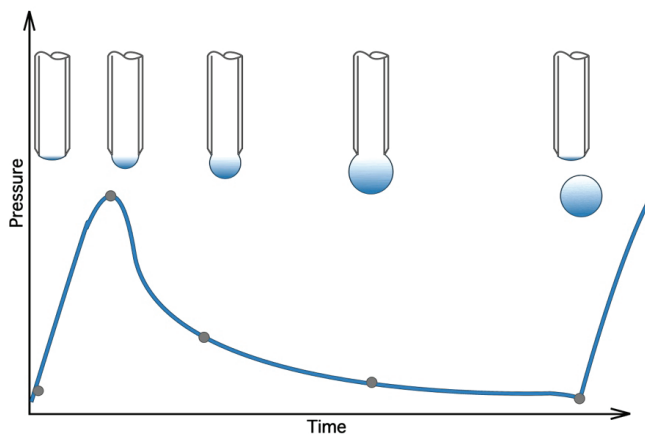


Figure 3.2. Pressure change in forming bubble (based on: Biolin Scientific, Attension Theory Note 2)

Optical Tensiometry (Theta)

Static surface tension of air/liquid interface can be measured with the pendant drop method (Cheng et al., 1990). The Theta optical tensiometer allows measurements with droplets and also with bubbles. The tensiometer was provided by Attension (formerly KSV Instruments).

The Theta coupled with a pulsation drop module (PD-200) enables measuring the long-term dynamic surface tension of air/liquid interface. During the term the bubbles are oscillated with 0,7 Hz frequency to impose dynamic conditions. The time dependency of surface tension is monitored up to minutes. The long-term dynamic surface tension (γ_{dl}) is determined from the shape factors of the bubble/droplet hanging from the tip of the needle:

$$\gamma_{dl} = \frac{\Delta\rho g R_0}{\beta} \quad (\text{Eq. 3.2})$$

where β is the shape factor calculated with the Young-Laplace equation (Girault et al. 1984, Hansen and Rodsrud, 1991).

Surface pressure measurement

Adsorbed surface-active agents decrease the surface tension due to the monolayer formation at air/liquid interface. The magnitude of decrease in

surface tension related to the one measured in pure system (γ_0) determines the surface pressure (Π):

$$\Pi = \gamma_0 - \gamma \quad (\text{Eq. 3.3})$$

The lower the surface coverage the higher the distance between the adsorbed molecules hence the surface pressure is lower. Surface pressure increases when the distance between the adsorbed molecules decreases.

Langmuir-Blodgett Trough (LBT)

Distance between molecules can be reduced with the contraction of surface area. Molecules exert a repulsive effect on each other when the active area of the air/liquid interface is reduced leading to increase in surface pressure (Figure 3.3). Barrier system is employed to control the active surface area in the LBT. The LBT used during the present study was produced by KSV NIMA (formerly KSV Instruments and Nima Technology).

The LBT has been traditionally designed to characterize the rheological properties of insoluble monolayers at air/liquid interface. However, during the present study water-soluble frothers were employed therefore the reduction of active surface area did not necessarily cause increase in surface pressure due to the possibility for molecule desorption. The change in surface pressure induced by the contraction and extension of the active surface area gives a hint of adsorption/desorption properties of the interface. The measurements were done in 250 ml sample solutions after 20 minutes of relaxation time. The speed of the barriers used to first contract and then extend the active surface area was set to 50 mm/min.

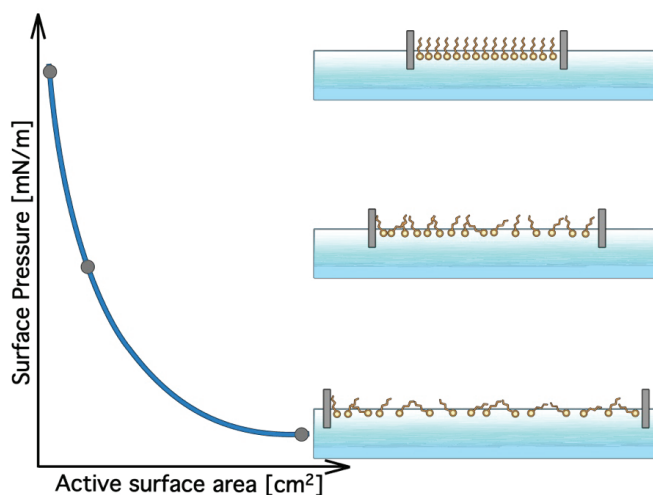


Figure 3.3. The effect of surface area reduction on the ordering of molecules at air/liquid interface (based on: Biolin Scientific, KSV NIMA Glossary)

Wilhelmy plate is employed to measure the Π of the active surface area (Wilhelmy, 1863). The plate immersed into the liquid phase indicates the change in surface tension calculated with the Wilhelmy equation:

$$\gamma = \frac{F}{L \cdot \cos\theta} \quad (\text{Eq. 3.4})$$

where F is the force on the plate, L is the immersed perimeter of Wilhelmy plate and θ is the contact angle between the liquid and the plate. The results obtained with LBT are introduced in **Publication IV and V**.

3.2.2 Study of air/liquid interface properties

Dilatation elasticity measurement

Interfacial rheology deals with the response of interfaces against deformation (Miller et al., 2010). The ability of the film to increase tension during deformation is called surface elasticity as defined by Gibbs (1948):

$$E_G = \frac{2 \cdot d\gamma}{d \ln A_s} \quad (\text{Eq. 3.5})$$

The Gibbs elasticity is valid only when the air/liquid interface is in equilibrium with the bulk phase under deformation. In non-equilibrium condition the Marangoni or dynamic surface elasticity is applicable (Malysa, 1981). The non-equilibrium state of the interface could be caused either by distortion of the equilibrium state or the absence of equilibrium (Malysa and Lunkenheimer, 2008).

The dynamic surface elasticity contains not only the pure elastic contribution or storage modulus (E') but also the viscous contribution or loss modulus (E'') (Lucassen-Reynders, 1981):

$$E = E' + iE'' \quad (\text{Eq. 3.6})$$

The E'' contains the true surface viscosity parameter (η) the measure of energy dissipation into heat (Lucassen-Reynders and Lucassen, 1994).

$$E'' = 2\pi\nu\eta \quad (\text{Eq. 3.7})$$

Optical tensiometry coupled with pulsation drop module (Theta + PD-200)

Bubble oscillation method was employed to investigate surface dilatation viscoelasticity property of air/liquid interface in presence of flotation frothers. The method introduced by Lunkenheimer and Kretzschmar (1975) uses harmonic interfacial disturbance to measure the elasticity of the interface.

Theta optical tensiometer coupled with PD-200 was employed to measure the dynamic elastic properties of the disturbed air/liquid interface. The PD-200 module is designed by Attension (formerly KSV Instruments) in order to measure dilatation viscoelasticity with the Theta optical tensiometer. Bubbles are formed into the test solution via a hooked stainless steel capillary and monitored for 20 minutes. The bubbles are oscillated during the measurement with the regulated frequency of 0,7 Hz. Surface oscillation is started



immediately after bubble formation without sufficient relaxation time required to reach equilibrium surface coverage; therefore the whole measurement is made in non-equilibrium conditions.

A high speed FireWire camera (Basler A602f) fitted with a 55 mm Telecentric lens (Computar TEC-M55) is employed to capture the behavior of bubbles during oscillation. The dynamic dilatation elasticity (E' and E'') of the air/liquid interface is calculated based on the recorded videos by the OneAttention software. The dilatation elasticity results are reported in **Publication IV and V**.



3.2.3 Study of bubble properties

The change of air/liquid interface properties affects the behaviour of air bubbles in dynamic two-phase systems. Bubble rising velocity and bubble breakup measurements were employed to investigate the bubble properties in dynamic two-phase system in the presence of flotation frothers. The bubble generation processes employed during the bubble rising and breakup measurements were alike, thus they are introduced together in the following subchapter.

Bubble generation

Glass capillaries with the inner diameter of 0.25 mm were used for bubble generation with various airflow rates. The only exception is the *bubble rise velocity column* (BRVC) where steel capillary with 0.26 mm inner diameter is employed for bubble generation.



Figure 3.4. Picture of bubbles formed with highest airflow rate

At the lowest airflow rate the bubbles are formed with sufficient time lag to avoid coalescence or collision in static conditions. The increasing airflow rate leads to an increase in the frequency of coalescence already during the formation of bubbles; nevertheless, the airflow rate never becomes high enough to form jet (Figure 3.4).

The size of the created bubbles fluctuated between 2.1 and 2.8 mm.

Bubble rising velocity measurement

In the first stage of bubble rise, the bubbles accelerate quickly and reach their maximum velocity from the initial zero within milliseconds (Sam, 1995). The maximum velocity is determined by the shape of the bubble changing as the results of molecule adsorption (Maldonado et al., 2013). Monitoring the rapid change of surface property during the early-stage of bubble rise is challenging but crucial for understanding the mechanism of frother action on bubble properties. High speed imaging technique and two bubble rising columns were employed during this study.

High speed imaging

Fastcam SA1 with a resolution of 640x1008 pixels and frame rate of 5000 fps was employed to monitor the early-stage of the bubble rise. Five videos were recorded with each frother concentration. *Matrox Inspector* image analysis software was used to analyse the horizontal- (D_h) and vertical diameter (D_v) of the bubbles with ellipse fitting method. The measured quantities were used to calculate D_{eq} based on Hernandez-Aguilar et al., (2005):

$$D_{eq} = \sqrt[3]{(D_h^2 \cdot D_v)} \quad (\text{Eq. 3.8})$$

Bubble rising velocity column (BRVC)

The BRVC was designed to monitor the early-stage of bubble rise and to measure the dynamic surface tension of the solution at the same time. The schematic of the experimental set-up is plotted in Figure 3.5. It consists of a square based glass sample vessel immersed into a thermostated acrylic bath. The monitored bubbles are formed in the sample vessel by the BPA-800P tensiometer.

The bubbles were created with a hook shaped steel capillary and the lifetime of the bubbles was controlled by the BPA. The bubble lifetime of each recorded bubble was 0.1s independently of the type and/or concentration of the frother solution therefore the available adsorption time of molecules was equal in each frother solution. Note that, high viscosity difference between sample solutions can cause differences in bubble size. In the present work, such phenomenon was observed in very highly concentrated, 7000 ppm DF200 solution, where the bubble size was around 2.1mm instead of the average 2.5mm observed in the rest of the frother solutions. The experimental set-up is first introduced in

Publication I. and the setup is also employed during the measurements introduced in **Publication II.**

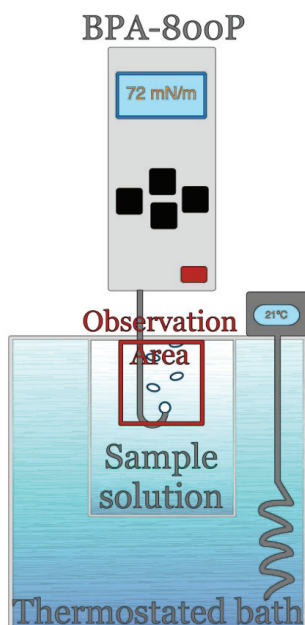


Figure 3.5. Schematic of bubble rising velocity column (BRVC)

Split bubble rising column (SBRC)

The SBRC is designed for the purpose of monitoring early-stage of bubble rise in the absence of momentary shock on the bubble surface caused by capillary detachment. The schematic of the experimental setup is plotted in Figure 3.6.

The square based rising column is divided into two well-separated sections. The lower section filled with ultra pure water is used to generate the bubbles. The upper section filled with sample frother solution is employed to monitor the rising velocity of the bubbles. A rotating valve installed between the two sections is the only access point from the lower part to the upper. The rotating valve is made out of a round steel bar. A hemisphere cavity is shaped in the steel bar with the size suited for ushering one bubble from the lower section to the upper section. The optimized size of the cavity minimizes the amount of liquid, which could be transmitted from one section to the other, when the bubbles are escorted to the upper section. Consequently, the solutions in the two sections are not mixed significantly.

The new release technique provides a more accurate method for monitoring the deviation in rising velocity caused by molecules adsorption at early-stage of bubble rise. This new experimental idea is first introduced in **Publication II.**

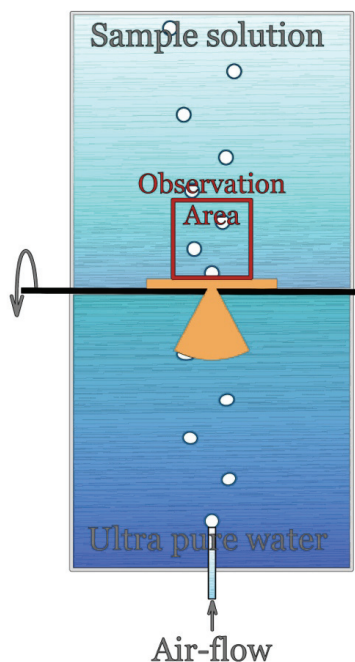


Figure 3.6. Schematic of split bubble rising column (SBRC)

Bubble breakup measurement

The chemical structure of molecules influences the stability of air/liquid interface; consequently, determines the size of maximum stable bubble under dynamic conditions (Walter and Blanch, 1986). High-speed imaging technique and the McGill cell were employed to study the effect of frothers on the bubble breakup caused by turbulent eddies.

High speed imaging

Bubble formation and bubble rising in the *McGill cell* is monitored with the *Fastec Trouble Shooter* (Model: TSHRMS) camera. The high speed imaging equipment was operated with the resolution of 1280x512 pixels and with 1000 fps rate.

Three videos were recorded with each concentration. The recorded videos were analysed with *ImageJ* software and the D_{eq} was determined.

McGill cell

The McGill cell was designed by Kracht and Finch in 2009 with the purpose of investigating the breakup properties of bubbles under dynamic conditions. The same set-up was used in the present study but some minor changes were made in order to guide the bubbles into the observation areas. The cell was a 30 l rectangular based acrylic tank with a pointed end glass capillary installed at the bottom of the tank (Figure 3.7). Bubbles formed via the glass capillary

were monitored via the observation area I. Bubble formation measurements were carried out in static conditions. Observation area I covered the track of the bubbles from the point of detachment till the height of 115 mm.

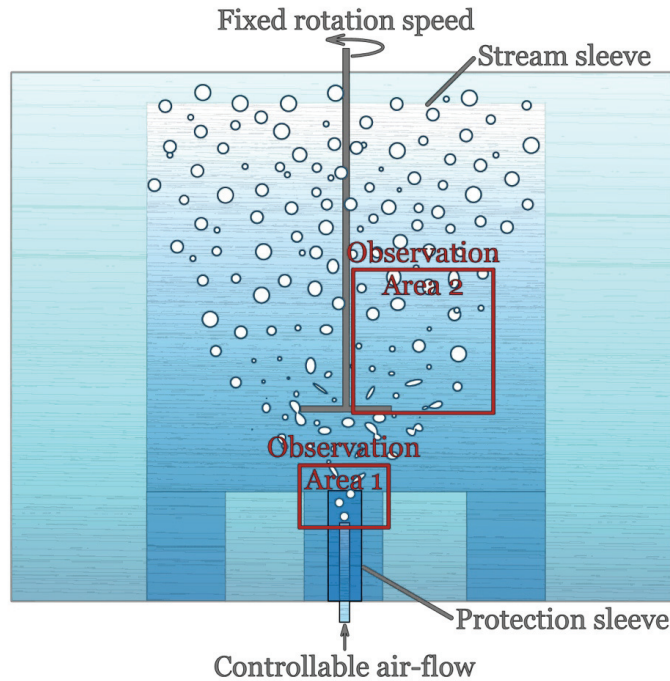
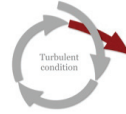


Figure 3.7. Schematic of the McGill cell employed to monitor bubble breakup

Observation area II was used to monitor the rising bubbles in dynamic conditions. A three-bladed axial flow impeller, with the rotation speed of 420 rpm, was installed about 5 mm above the capillary in order to develop turbulent flow in the cell. The three-bladed axial flow impeller and its rotation speed corresponded to that used by Kracht and Finch (2009). An acrylic sleeve around the capillary protected the forming bubbles from eddies created by the impeller; therefore the size of the forming bubbles in dynamic conditions was similar to that observed in static conditions. Another sleeve around the impeller prevented the dispersion of monitored bubbles and guided them into the observation area II.

The difference in the measured bubble size between the two observation areas gave indication on the effect of frothers on bubble breakup. The size of forming bubbles was controlled by the airflow rate varied between 15 and 35 sccm. Sierra 840D-L-1-VI mass flow controller regulated the airflow during the bubble formation. The breakup properties of bubbles in the presence of flotation frothers are reported in **Publication V**.



3.2.4 Study of bubble-bubble interaction properties

Bubble coalescence measurements

The contact time required for bubbles to coalesce becomes longer in the presence of flotation frothers (Saghert et al., 1976) as the results of the increase of drainage time (Machon et al., 1997). The drainage time increases with increasing surface tension gradient and decreasing surface mobility (Pugh, 1996). However, the approach speed of the bubbles also affects the bubble coalescence (Yaminsky et al., 2010) that makes crucial investigating the coalescence property of bubbles in turbulent conditions. High speed imaging technique and the shear flow observation chamber were used to investigate this behaviour.

High speed imaging

Two digital video cameras were used to monitor the coalescence of bubbles under dynamic conditions. High speed *Fastcam SA1* with the resolution of 640x1008 pixels and the frame rate of 5000 fps captured the bubble formation. Progressive scan monochrome camera (*JAI CV-M10 SX 1/2"*) with 25 fps rate observed the rising bubbles.

Three videos per frother concentration were recorded with each camera. The D_h and D_v of bubbles were calculated with the *ImageJ* software in order to determine the D_{eq} based on Hernandez-Aguilar et al., (2005). The difference in D_{eq} observed with the two cameras gave indication of the effect of frothers on bubble coalescence under dynamic conditions.

Shear force observation chamber (SOC)

The SOC is an acrylic flow chamber (Figure 3.8) that allows sampling the same batch of bubbles at their creation point and later, during the bubble rising. The SOC can be divided into two parts based on their function: the “tunnel” and the “chimney”.

The tunnel is a square based (5x5 cm) flow chamber with the length of 40 cm. Three glass capillaries, with the inner diameter of 0.25 mm, protrude through its bottom. The capillaries are placed at 9 mm distance from each other in order to prevent coalescence between the adjacent bubbles during formation. There is a turbulence creating obstruction placed 2.5 cm ahead the capillaries in order to develop shear force affecting bubble formation. The bubble formation is monitored at the capillaries via the Observation Area I.

The chimney is a 40 cm tall open-top column, where the flow velocity decreases creating quiescent conditions and the bubble rising is monitored via the Observation Area II. The sample solution is circulated back from the chimney into the tunnel with a *LPP-D 25 peristaltic pump* (Larox Flowsys Oy) via a pulsation damper.

The *GFC mass flow controller* (Aalborg Instruments & Controls, Inc.) controls the airflow rate used for bubble generation. The size of the generated bubbles is varied with the airflow rate (the increase of airflow rate increases the bubble size already during the formation) between 2.1 and 2.8 mm.

Four parameters are varied during the study viz. composition of the medium (frother type and concentration), dynamic properties of the medium (presence or absence of turbulence), size of the created bubbles by *GFC mass flow controller* and the number of capillaries used for bubble generation.

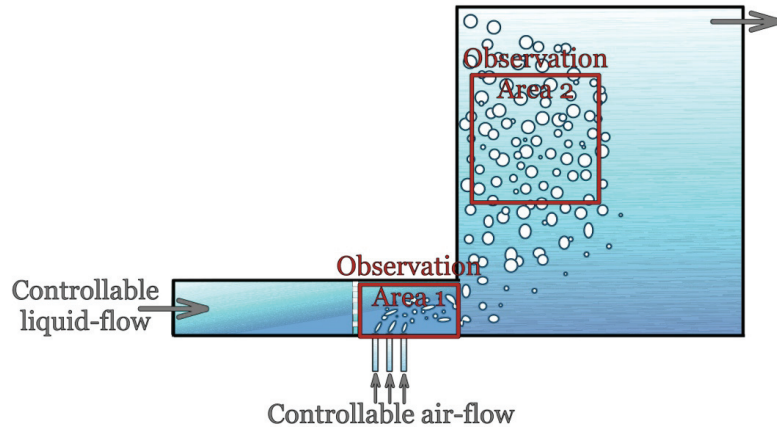
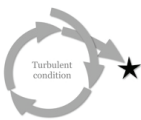


Figure 3.8. Schematic of shear force observation chamber (SOC)

The experiments were performed at 0, 3, 8, 16, 25, 50 and 100 ppm frother concentrations where the temperature of the solution was 21 °C. The SOC is first introduced at the XXVI International Mineral Processing Congress and also in **Publication III**.



★ 3.2.5 Study of bubble size in mechanical flotation cell

Image recording and data analysing

The size of the bubbles in the quiescent zone of the mechanical flotation cell was monitored with the Nikon D90 digital camera. The camera exposure settings were: ISO 1250, Aperture F6.3, Shutter speed 4000 (1/4000 second). The picture series were taken using the burst-shooting mode of the camera (1 picture per second) for a timed period of 105 seconds. Figure 3.9 shows the bubble samples captured in water and in 8 ppm DF250 frother solution.

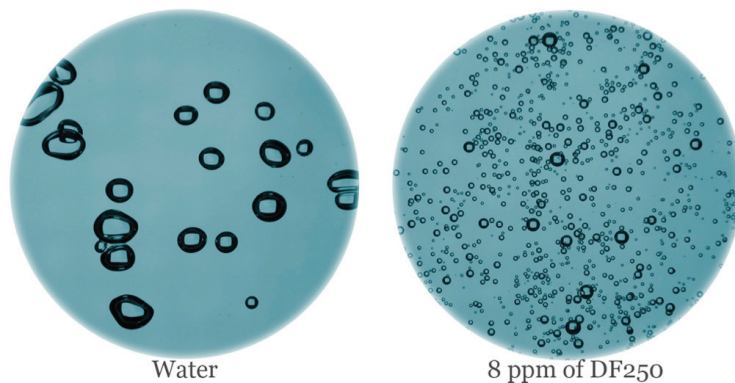


Figure 3.9. Bubble samples collected with MBSA in water and in 8 ppm of DF250

Three sets of measurements were repeated and recorded with each frother solution. *ImageJ* software with ellipse fitting method was used to determine the d_h and d_v of bubbles to calculate D_{eq} and D_{32} .

The 3-parameter model, introduced by Nasset et al. (2007), was used to fit the Sauter mean-concentration (D_{32} -C) isotherm on the measured data points and estimate the CCC95:

$$D_{32} = D_L + A \cdot \text{Exp}\left(-b \cdot \frac{c}{\text{CCC95}}\right) \quad (\text{Eq. 3.9})$$

The CCC95 is the concentration causing 95% reduction in D_{32} compared to that in water alone (Hernandez-Aguilar and Finch, 2005).

Sauter mean diameter measurement

Mechanical flotation cell

The measurements were made in the *OK-265* laboratory flotation cell. The Plexiglas OK cell is a 265 dm³ open-top cylindrical box ($d_{\text{cell}} = 0.65$ m) designed by Outotec (formerly Outokumpu Technology). Grau and Laskowski (2006) described the cell in detail. The D_{32} results observed in the OK cell are reported in **Publication III – V**.

McGill bubble size analyser (MBSA) was employed to capture bubbles from the quiescent zone of the cell (Hernandez-Aguilar et al., 2002). The concentration of the solution in the MBSA and in the flotation cell was set separately. The concentration in the MBSA was 40 ppm during the whole study to prevent coalescence inside the bubble sampling tube. The concentration of frother in the flotation cell ranged between 0 ppm and 40 ppm and the measurements were performed at 14 different concentration points.

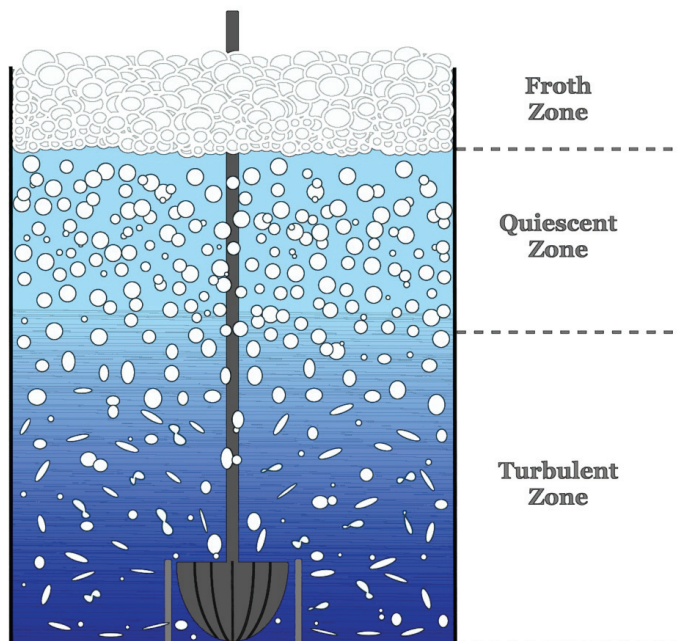


Figure 3.10. Schematic of mechanical flotation cell and the three distinct zones within the cell

The *Multi-Mix* rotor/stator mechanism produced by Outotec dispersed and agitated the air in the frother solution (Figure 3.11). The rotor tip speed (S) and superficial gas velocity (J_g) were 4.7 m/s and 0.5 cm/s respectively. The tip speed was determined based on the rotor diameter ($D_{rot} = 0.15$ m) and the revolutions per minute (N):

$$S_{rot} = \pi \cdot N \cdot D_{rot} \quad (\text{Eq. 3.10})$$

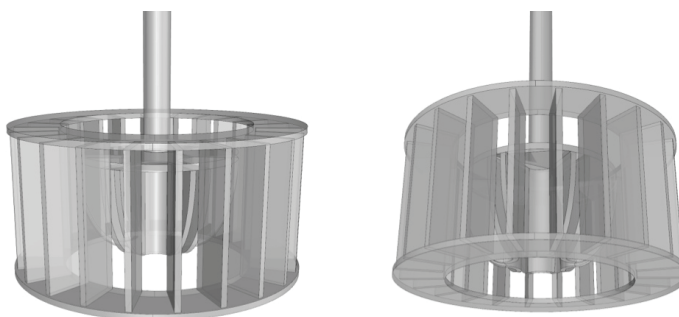


Figure 3.11. Schematics of *Multi-Mix* rotor/stator mechanism (pictures courtesy of Mr. Juha Tiitinen)

4. Evaluation of the measurement data accuracy

This chapter introduces the accuracy of the applied measurement methods in detail. Each size-scale measurement is discussed in a separate sub-chapter.



4.1 Evaluation of micro/nano-scale data

All laboratory equipment used for studying dynamic micro/nano-scale phenomena were provided by Attension and by KSV NIMA (formerly KSV Instruments). Each instrument possesses its own software used for data analyses.

The accuracy of the measurements is determined by the accuracy of the laboratory equipment and its own software (specified by the manufacturer), the calibration of the equipment, and the cleanness of the laboratory glassware, equipment and tools used during sample preparation and measurements. The calibration was always made in ultra pure water and repeated each time, when the instrument were moved or spare parts were changed. A test measurement was always performed in ultra pure water, on each measurement day, before the actual measurements started in order to check if the instrument is in good working condition.

The cleaning procedure of the laboratory glassware and tools consisted of four major actions: pre-washing, washing, rinsing and final rinse. The pre-washing was made by brush under running tap water in order to eliminate the major contaminations. The Branson 5510 ultrasonic cleaner was used for the washing process. The cleaner was filled up with the mixture of pure water and RBS (T 105) laboratory detergent. The operation temperature was 60°C and the sonication time was 60 min. After the washing every piece of equipment was rinsed separately, with pure water, at least three times. In the final rinse all the glassware and tools were soaked and rinsed with ultra pure water.

The measurements with each frother solution was repeated three times and the final results were calculated as an average of the three repetitions. The following list summarises the major actions performed during laboratory measurements:

- Executing the measurement with the particular frother solution in a condition specified by the user.
- Saving the measured data and analysing it with the software provided by the manufacturer.
- Repeating the measurements three times and transferring the data into an excel file. Calculating the average and the standard deviation of the results.

An example of the average results calculated based on three measurements are shown in Figures 4.1-4.3. The γ_{ds} results measured with BPA-800P are plotted in Figure 4.1. Due to the high accuracy of the equipment, the proper calibration and the extensive cleaning process the standard deviation is low (± 0.1 mN/m) implying high reproducibility during the short-term dynamic surface tension measurements. The results of dynamic surface tension measurements are summarized in **Chapter 5.1** and introduced in more detail in **Publication I, II, IV, V and VI**.

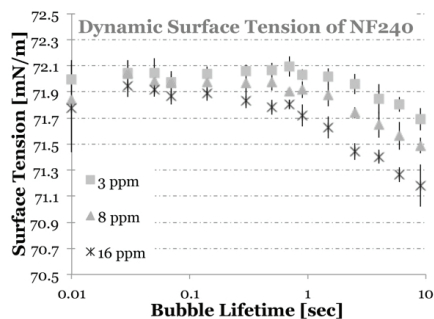


Figure 4.1. The reproducibility of the short-term dynamic surface tension results measured with BPA-800P in NF240 solution

The surface pressure results obtained with LBT suggest a higher standard deviation (± 0.9 mN/m) with increasing frother concentration; nevertheless, even with high frother concentration the results are still well reproducible (Figure 4.2). More detail about the effect of effective surface area on surface pressure is introduced in **Chapter 5.1** and in **Publication IV-VI**.

The data measured with Theta+PD-200 shows well reproducible long-term dynamic surface tension results (Figure 4.3a) however the viscoelasticity results are less precise due to the relatively high standard deviation (Figure 4.3b). The high standard deviation is caused most likely by the high sensitivity of the instrument where even the smallest perturbation could cause a high standard deviation. These deviations are not persistent therefore the viscoelasticity results are shown with their standard deviation here and later on in **Chapter 5.1** and in **Publication IV-VI**.

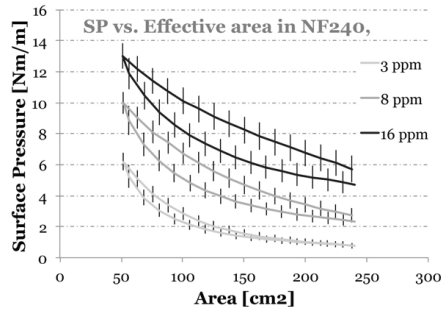


Figure 4.2. The reproducibility of the surface pressure results observed with LBT in NF240 solution

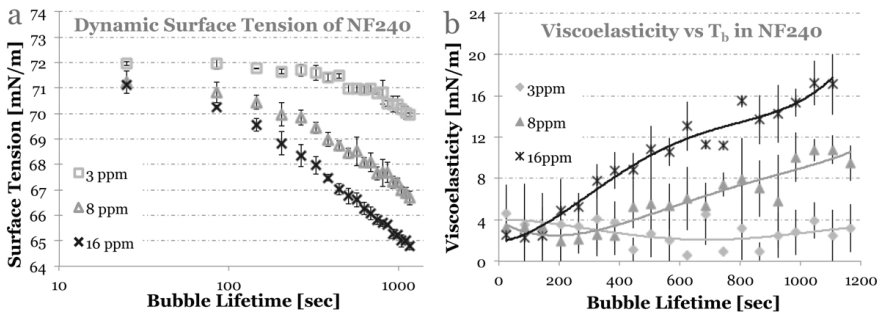


Figure 4.3. The reproducibility of the results measured with Theta+PD200: a) during long-term dynamic surface tension data analyses, b) during dilatation elasticity data analyses in NF240 solution



4.2 Evaluation of meso-scale data

The experimental set-ups used to monitor dynamic meso-scale phenomena were designed and built at Aalto University, Finland. The only exception was the *McGill cell* designed and built at McGill University, Canada.

The experimental set-ups used during meso-scale studies are very large and complex compared to laboratory equipment introduced in the previous subchapter. Consequently, there are numerous additional factors determining measurement accuracy, such as the cleanness of the set-ups (due to the complexity and size of the set-ups the cleaning process is difficult), the quality of the sample solution (the large quantity makes the dilution process challenging), the sampling technique (the number of sampled bubbles and the size of the sampling area is a crucial factor), the quality of the captured images (that will have a significant effect on the results obtained during image analyses) and the accuracy of the additional equipment employed to create dynamic condition into the observation chambers.

Reference measurements were performed daily with pure water before the actual measurements started. At the end of the measurement days the set-ups

were cleaned with *Nalgene L900* liquid detergent (except the McGill cell that is cleaned with ordinary dish soap) and rinsed with pure water. The test solutions were prepared with high degree of caution to avoid any errors. The image analyses process is reported in detail in Chapter 4.4. The sampling technique and the accuracy of the experimental set-ups vary according to complexity of the equipment. These parameters of the set-ups are introduced individually in separate sub-chapters (Chapter 1.2.1-1.2.3).

The major actions performed during the meso-scale measurements are summarised in the following list:

- Rinsing the set-up with pure water and making the equipment ready for reference measurement performed in pure water.
- Adjusting the camera and the lights in order to get a perfectly sharp picture quality and good contrast.
- Setting the condition of the media specified by the user and waiting 2 to 5 minutes until uniform conditions are reached.
- Taking the reference measurement.
- Adding the frother (or the prepared sample solution in case of bubble rising study) and mixing it well for 3 to 5 minutes.
- Executing the measurement and repeating three times (5 times in case of bubble rising study).
- Saving the captured pictures and cleaning the set-up before new measurements are performed.
- Analysing the data with image analysing software (more detail in Chapter 4.4) and transferring the data into an excel file. Calculating the average and the standard deviation of the results.

4.2.1 Accuracy of the bubble rising velocity study

Figure 4.4 shows the average of bubble rising velocity (a) and the average of aspect ratio (b) obtained in BRVC. The average, resulting from five repetitions, shows low standard deviation (± 0.1 cm/s) thanks to the extensive cleaning process, the high quality of pictures and the simple sampling technique. The bubble sampling technique applied during bubble rise studies is a straightforward method, where the property of each created bubble is easily traceable.

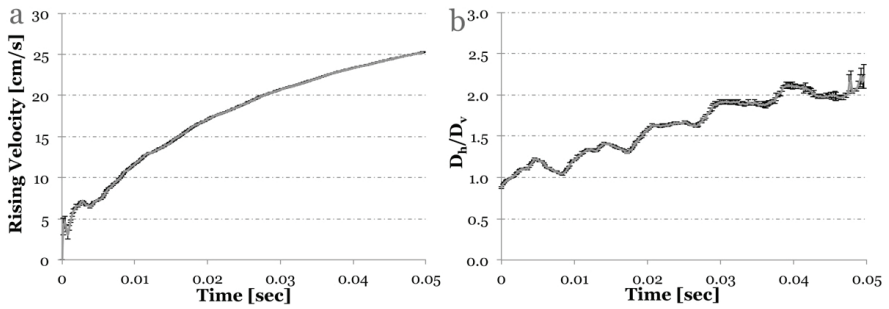


Figure 4.4. The reproducibility of a) bubble rising velocity; and b) aspect ratio results obtained in BRVC. The plotted results are measured in NF240 solution

The bubble rising velocity observed in SBRC also showed low standard deviation even at late-stages of bubble rise (Figure 4.5a). Nevertheless, the aspect ratio results show a higher standard deviation, especially at late-stage, but the trend is still apparent. The rising velocity results are introduced in more detail in **Chapter 5.2** and in **Publication I** and **II**.

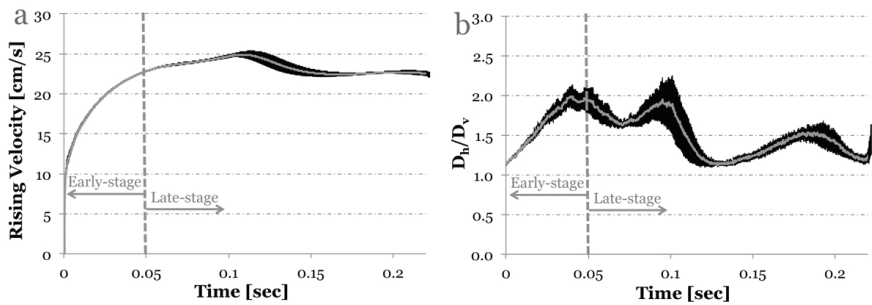


Figure 4.5. The reproducibility of the early-stage and late-stage a) rising velocity; and b) aspect ratio measurements observed in SBRC. The plotted results are measured in NF240 solution

4.2.2 Accuracy of the bubble breakup study

Two observation areas were employed to monitor the bubble properties in the McGill cell. The size of the forming bubbles was monitored via the Observation area I. (Figure 4.6), while the bubbles passing through the dynamic medium were monitored via Observation area II. The difference in bubble size detected between Observation area I., and Observation area II., determines the breakup properties of bubbles in presence of frothers. The employed bubble sampling techniques differ in the two areas.

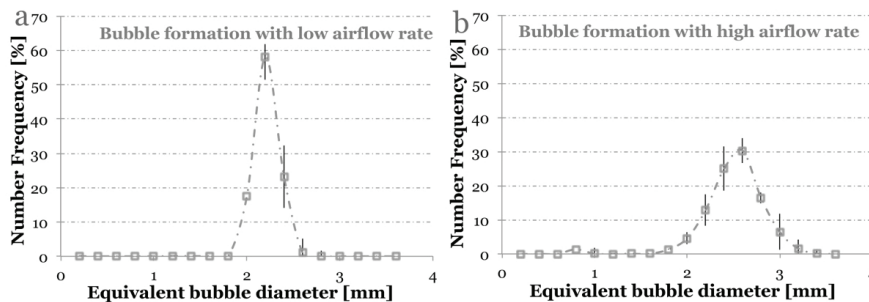


Figure 4.6. Size distributions of the bubbles formed in steady-state condition a) with low airflow rate (15 sccm) and b) with high airflow rate (35 sccm). (The error bars represent the standard deviation based on three repetitions observed in NF240)

The properties of each forming bubble are easily traceable; therefore, the sampling method has a negligible effect on the accuracy of the bubble size measurement.

In the Observation area II., it is not perfectly feasible to monitor each bubble passing through the dynamic medium. In order to minimize bubble dispersion, a stream sleeve was installed around the impeller, whence most of the bubbles were escorted into the Observation area II. Figure 4.7 shows the standard deviation of the bubbles created with low airflow rate (15 sccm) and high airflow rate (35 sccm). The standard deviation of the bubble size observed in the Observation area II., can be much higher than that in Observation area I., as a result of the bubble sampling technique.

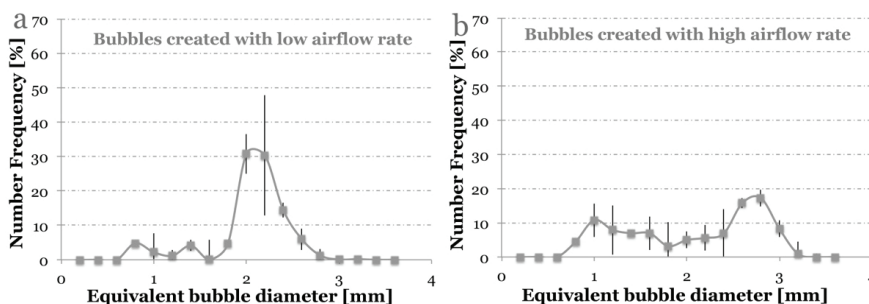


Figure 4.7. Effect of dynamic conditions on the size distributions of bubbles created a) with low airflow rate (15 sccm) and b) with high airflow rate (35 sccm). (The error bars represent the standard deviation based on three repetitions observed in NF240)

Surprisingly, the standard deviation of the bubble size is moderated when reagent grade agents are used instead of commercial frothers (Figure 4.8). The bubble breakup, in the presence of reagent grade agents and commercial frothers, is studied closely and the findings are summarized in **Chapter 5.2** and **Publication V**.

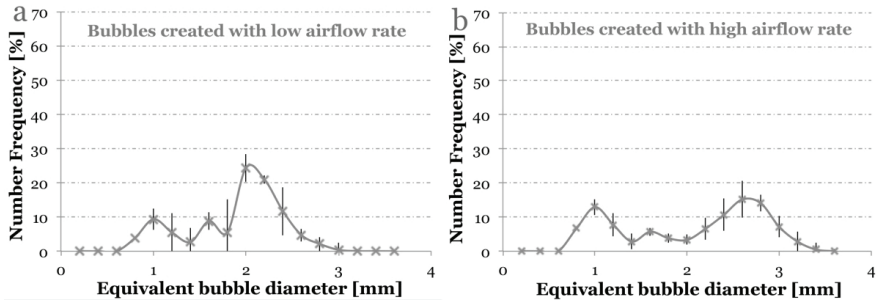


Figure 4.8. Effect of dynamic conditions on the size distributions of bubbles created in commercial I-Pentanol a) with low airflow rate (15 sccm) and b) with high airflow rate (35 sccm). (The error bars represent the standard deviation based on three repetitions)

4.2.3 Accuracy of the bubble coalescence study

Bubble interactions in dynamic conditions were studied in two observation areas, likewise the bubble breakup studies. The *forming bubbles* were monitored via Observation area I. Although each forming bubble is easily traceable, in some cases, the size distribution suggests extensive fluctuation of bubble size even in static conditions (Figure 4.9). The fluctuation is less outstanding when bubbles are created with three capillaries. The difference in imaging parameters (close-up view and high pixel resolution) employed during bubble formation study is the explanation for the high standard deviation.

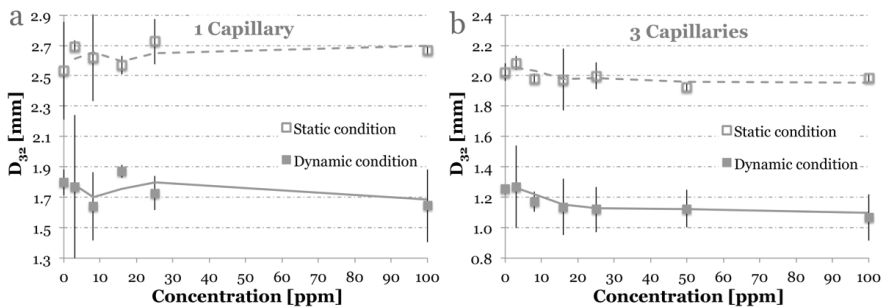


Figure 4.9. The reproducibility of the Sauter mean diameter measurement of forming bubbles formed with: a) one capillary or b) three capillaries in static and dynamic conditions. The plotted results are measured in NF240 solution

Images of *rising bubbles* in these measurements are captured over a broad area. As a result of the increased distance between the camera and the observation area, the standard deviation of D_{32} decreases significantly (Figure 4.10).

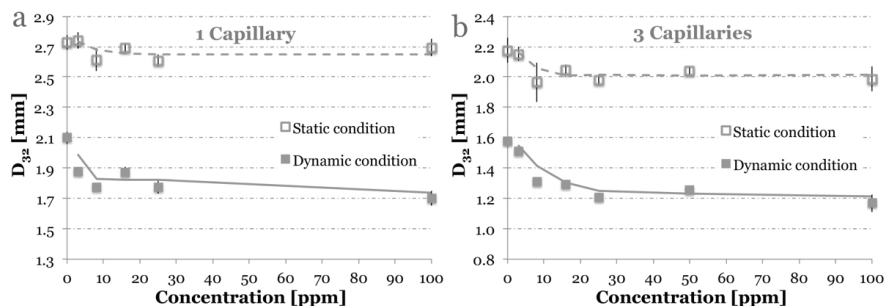


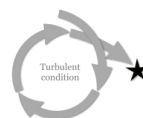
Figure 4.10. The reproducibility of the Sauter mean diameter measurement of rising bubbles formed with: a) one capillary or b) three capillaries in static and dynamic conditions. The plotted results are measured in NF240 solution

Despite the greater extent of Observation area II, it is not fully manageable to monitor each bubble passing through the dynamic medium especially when the bubble interactions are investigated in high frother concentration. This might affect the data observed in high frother concentration however it has no effect on the trend. More details about the frother effect on bubble coalescence obtained in turbulent conditions are introduced in **Chapter 5.2** and in **Publication III**.

4.3 Evaluation of macro-scale data

The size of bubbles dispersed in mechanical flotation cell was monitored in the OK-265 cell. The bubbles were sampled from the 265 dm³ cell, with the MBSA, 15 cm below the medium surface. The major actions performed during flotation cell test measurements are listed below:

- Cleaning the experimental setup with L900 plastic cleaning solution.
- Filling up the cell with tap water to 65 cm in height. Setting the position of MBSA filled up with 40 ppm frother solution.
- Setting the impeller speed to 600 rpm and the airflow rate to 100 l/min followed by 15 minutes conditioning time.
- Adjusting the camera and the lights in order to get a perfectly sharp, high contrast image.
- Removing the cork from the end of the sampling tube and taking 105 pictures using burst-shooting mode (1 picture/sec).
- Replacing the cork and adding frother to the tank. Repeating the measurement after 15 minutes of conditioning time (the concentration of the frother solution is increased from 0 ppm to 40 ppm and measurements are performed at 14 concentration points during the study of one frother).



- Saving the captured pictures and cleaning the set-up before new frother is tested.
- Analysing the data with image analysing software (more detail in Chapter 4.4) and transferring the data into an excel file. Calculating the average and the standard deviation of the results.

The average results calculated based on three sets of D_{32} measurements are shown in Figure 4.11. Although the experimental set-ups used during macro-scale studies are very large and complex, the reproducibility of the measurements is high and the standard deviation is very small (always below ± 0.1 mm). Bubbles are captured from the quiescent zone of the cell that minimizes the standard deviation and the elaborate cleaning procedure also has a significant effect on the high reproducibility of D_{32} measurements.

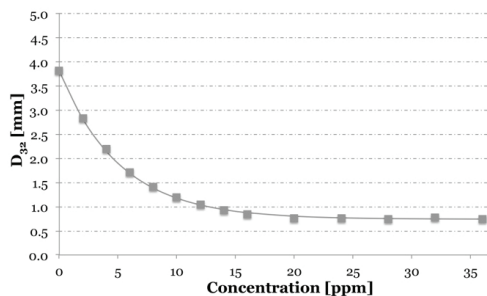


Figure 4.11. The reproducibility of Sauter mean diameter observed in mechanical flotation cell

The results of dynamic surface tension measurements are summarized in **Chapter 5.3** and introduced in more detail in **Publication III, IV and V**.

4.4 Image processing and calibration

High-resolution pictures were captured during meso-scale (Figure 4.12-4.14) and macro-scale studies (Figure 3.9). The calibration measurements were made in pure water. Each picture includes an object with a well defined, permanent dimensions used as a reference size.

Figure 4.12 shows two sample pictures taken of bubbles moving through the BRVC (a) and the SBRC (b). Fastcam SA1 was employed to monitor the bubbles with the resolution of 640x1008 pixels and frame rate of 5000 fps.

Each recorded video was analysed with Matrox Inspector Interactive Imaging Software. The capillary used for bubble generation and the edge of the transmitter orifice was used to calculate the actual pixels/mm ratio of each picture. The high picture quality, the sharp contrast and the relatively low surface perturbation (compared to dynamic conditions) made the picture

analysing process relatively easy and precise. The change in horizontal (d_h) and vertical diameter (d_v) of the bubbles was calculated with high accuracy.

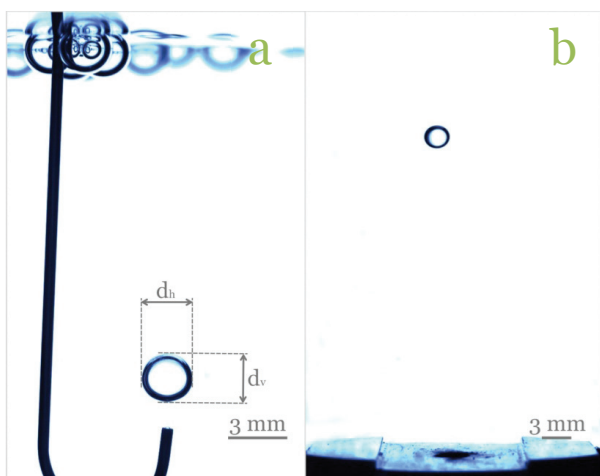


Figure 4.12. Sample pictures of bubble rising captured in a) BRVC and b) SBRC

The Fastec Trouble Shooter camera monitored the breakup properties of bubbles with the resolution of 1280x512 pixels and the frame rate of 1000 fps records 300 pictures per measurement. Figure 4.13 shows sample pictures of forming (a) and rising bubbles (b). The capillary and the shaft of the impeller were used to calibrate the actual pixels/mm ratio.

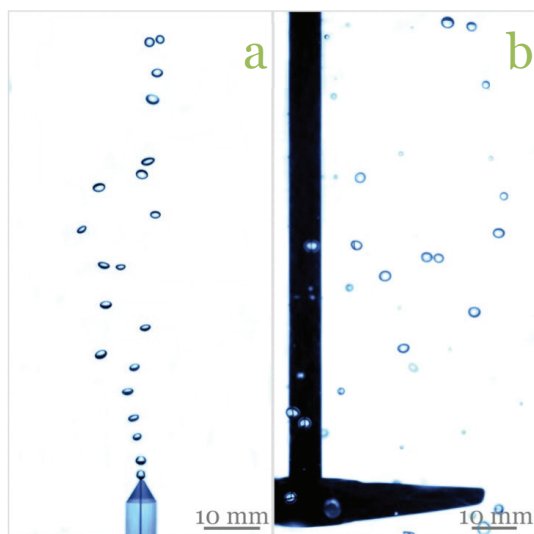


Figure 4.13. Sample pictures of bubble breakup properties captured in McGill cell via a) observation area I, and b) observation area II

The ImageJ software was employed during the analysing process. The high picture quality and sharp contrast obtained in static condition (Figure 4.13a)

facilitate the calculation of bubble size with high accuracy. However, in dynamic condition the bubble size analyses is more challenging due to the shallow depth of field achieved with the AF Micro Nikkor 60 mm micro lens. The shallow depth of the field meant that the bubbles moving through the turbulent zone could easily get out of focus (Figure 4.13b).

The two observation areas used to study the coalescence of bubbles in dynamic conditions were equipped with different cameras. The forming bubbles were monitored with the Fastcam SA1 (Figure 4.14a), while the rising bubbles were followed with the JAI CV-M10 monochrome camera (Figure 4.14b). The same image analysing software (ImageJ) was used during video analyses.

Despite of the high image quality and sharp contrast it was challenging to analyse accurately the size of forming bubble due to the high surface oscillation caused by the turbulent eddies and the overlapping of bubbles as a results of high bubble population.

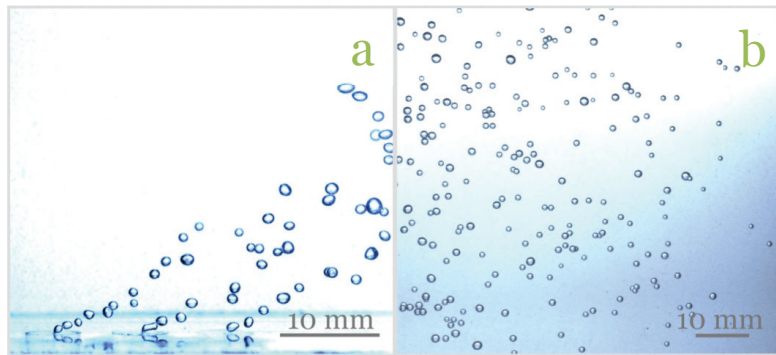


Figure 4.14. Sample pictures of bubbles interaction properties captured in SOC via a) observation area I, and b) observation area II

5. Main results and discussion

This chapter discusses the effect of frothers on the properties of the air/liquid interface under dynamic conditions. Each size-scale effect is introduced in a separate sub-chapter.



5.1 Micro/nano-scale results

Static surface tension as a function of frother concentration was investigated in the presence of three commercial frothers (DF200, NF240 and DF250). Figure 5.1a shows the static surface tension results obtained in the commercial frothers. The results shows that the DF250 is highly surface-active and decreases the surface tension effectively upon addition of small concentration while the DF200 is less surface-active; therefore higher frother concentration is required to diminish static surface tension to the same extent as DF250. Even though, the frothers eventually reach the quantitatively similar static surface tension, the dynamics of molecules adsorption differs (Figure 5.1b).

The dynamic surface tension was investigated at the frother concentration where the static surface tension was 61 mN/m. The dynamic surface tension results indicate different adsorption rates between the less surface-active DF200 and the two other frother solutions; therefore, the adsorption properties of the five studied surfactants was investigated in more details.

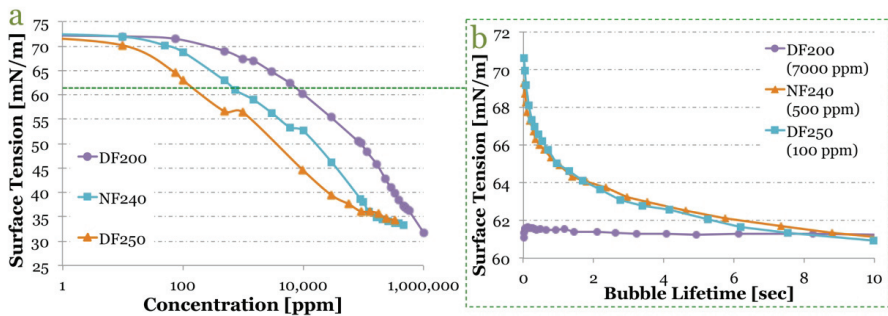


Figure 5.1. a) Static surface tension as a function of frother concentration and b) dynamic surface tension at equivalent static surface tension (61mN/m) concentration

The effect of increasing frother concentration on dynamic surface tension as a function of bubble lifetime ($\gamma_d - T_b$ isotherm) is plotted in Figure 5.2 and 5.3. The $\gamma_d - T_b$ isotherms contain the results observed by two different devices: the BPA-800P (solid markers) and the Theta optical tensiometer coupled with PD-200 (hollow markers). A vertical dashed line plotted in the figures separates the two sets of data.

The dynamic surface tension results highlight two distinct adsorption properties viz. a rapid, time independent and a slow, time determined. The rapid, time independent results indicate that the adsorption mechanism is only controlled by diffusion and it is observed in presence of less surface-active 1-Pentanol and DF200 (Figure 5.2).

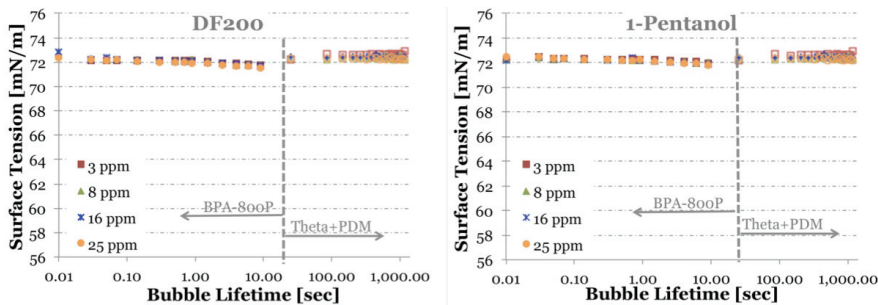


Figure 5.2. Concentration effect of short-chain surfactant on $\gamma_d - T_b$ isotherm obtained by BPA-800P (solid chart markers) and by Theta (hollow chart markers)

The slow, time determined results suggest diffusion-controlled re-arrangement of the already adsorbed surfactant. Time and concentration dependency of dynamic surface tension is significant in presence of highly surface-active PPG425 and DF250 (Figure 5.3).

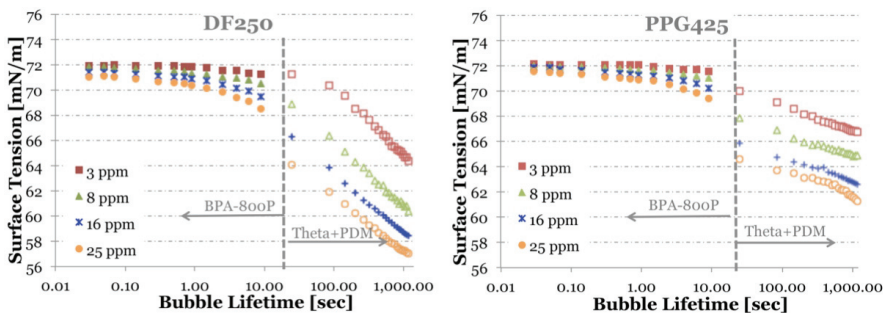


Figure 5.3. Concentration effect of long-chain surfactant on $\gamma_d - T_b$ isotherm obtained by BPA-800P (solid chart markers) and by Theta (hollow chart markers)

The rate and the hysteresis of adsorption/desorption were studied as a function of effective surface area with the LB Trough. The alteration of

effective surface area changes the surface pressure; however, the magnitude of the change is determined by the adsorption/desorption properties of surfactants. Therefore, even though a quantitatively identical initial surface pressure is reached before and after the compression/relaxation cycle in the two differing frother solutions, the similar alteration of effective surface area causes different surface pressure during the compression (Figure 5.4).

The effective surface area is varied with the barrier speed of 50 mm/min and during the first 160 sec the surface area is contracted and thereupon is extended. The peak of surface pressure – time (Π -T) isotherm observed in NF240 frother solution indicates a slow molecule desorption leading to a packed air/liquid interface; consequently, the surface pressure increases. In DF200 the change in effective surface area do not affect the surface pressure due to the rapid desorption rate therefore the Π -T isotherm is not changing as the function of surface area alteration.

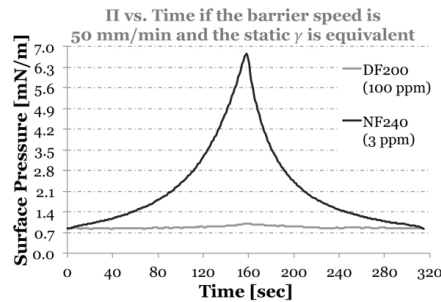


Figure 5.4. The effect of surface area change on surface pressure if the barrier speed is 50 mm/min and the initial Π is equivalent

The alteration of effective surface area does not cause perceptible change in surface pressure in the presence of less surface-active DF200 and 1-Pentanol due to the rapid diffusion controlled adsorption/desorption of molecules at the air/liquid interface (Figure 5.5.). This finding corresponds to that concluded based on the dynamic surface tension results.

The contraction of effective surface area induces increase in surface pressure in DF250 and PPG425 solutions (Figure 5.6). The surface pressure decreases during extension; nevertheless, there is a noteworthy hysteresis between the changes of surface pressure caused by contraction and by extension suggesting molecule desorption and re-orientation induced by interactions between molecules.

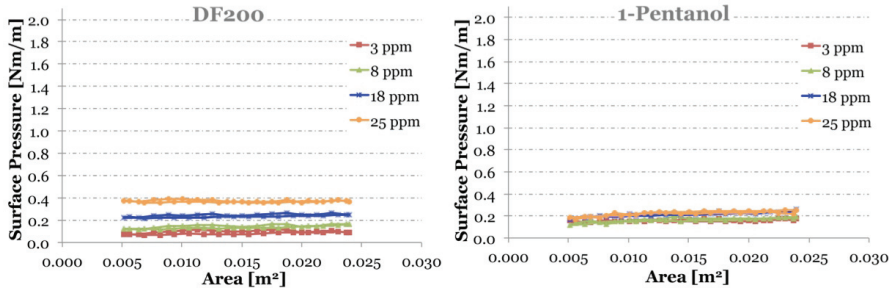


Figure 5.5. Surface pressure change determined by surface area variation in DF200 and 1-Pentanol frother solutions¹

The arrows in Figure 5.6 show the direction of the surface pressure drift. The difference between surface pressures observed in the initial stage and the final stage of the measurement suggests desorption.

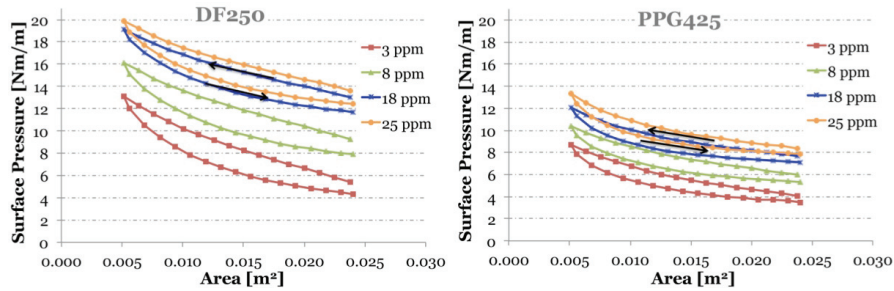


Figure 5.6. Surface pressure change determined by surface area variation in DF250 and PPG425 frother solutions

The dilatation elasticity of air/liquid interface is determined by the adsorption/desorption properties of the surfactants. In case of rapid diffusion controlled adsorption, observed in the presence of less surface-active DF200 and 1-Pentanol, the surface elasticity is below the measurement threshold of the instrument; therefore, the elastic property is not precisely detectable.

In highly surface-active PPG425 and DF250, the dependency of E (Eq. 3.6) on bubble lifetime and frother concentration is easily noticeable (Figure 5.7). Increasing frother concentration induces rise in surface elasticity and an increase in bubble lifetime further intensify the rise.

The change in dilatation elasticity of air/liquid interface is outstanding in DF250 solutions. The magnitude of change as a function of bubble lifetime decreases with increasing frother concentration. The concentration effect and also the time effect on dilatation elasticity are less remarkable in PPG425

¹ Note that the magnitude of the scale on the y-axis is ten times smaller in DF200 and 1-Pentanol than in case of the other surfactants.

meaning that even though the $\gamma_d - T_b$ isotherms suggest loading and re-orientating molecules, the elasticity remained constant.

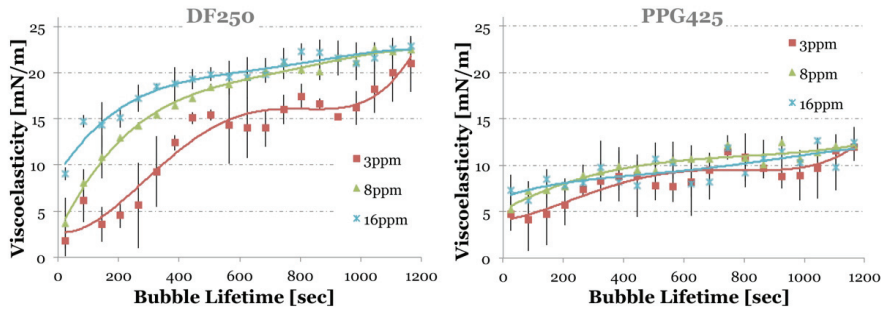
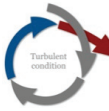


Figure 5.7. Time and concentration effect on dilatation elasticity (E) in DF250 and F150 frother solutions



5.2 Meso-scale results

5.2.1 Bubble rising velocity

The initial rising velocity of bubbles injected through a capillary into a highly diluted frother solution and into ultra pure water corresponds well. Figure 5.8 presents the initial rising velocity and aspect ratio of the bubbles in 8ppm of DF200 (Figure 5.8a) and DF250 (Figure 5.8b) as compared to the results observed in upw.

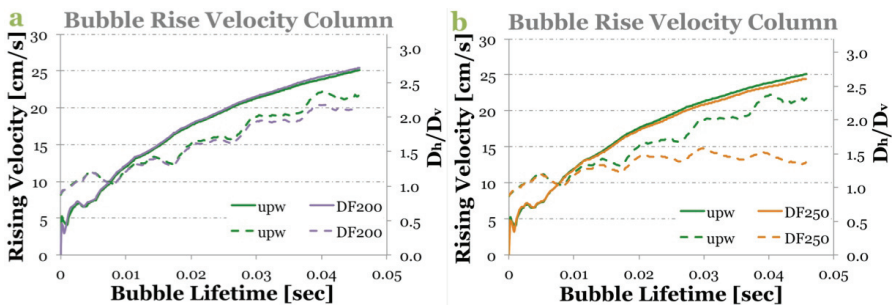


Figure 5.8. Rising velocity (solid line) and aspect ratio (dash line) of the bubble observed in BRVC a) in 8 ppm DF200; b) in 8 ppm of DF250

In 8 ppm DF200, the initial rising velocity and the aspect ratio of the rising bubbles show identical behaviour to the one observed in upw suggesting a mobile bubble surface. Kracht and Finch (2010) noticed similar surface mobility of the bubble surface in 1-Pentanol solutions. The aspect ratio results suggest a less mobile bubble surface in 8 ppm DF250 even though the early-stage of bubble rising velocity results does not indicate it. Low concentration

(≈ 5 ppm) of PPG425, also turns the bubbles surface stiffer, and consequently become less mobile (Kracht and Finch, 2010).

Bubbles released from the transmitter orifice of SBRC shows decrease in surface mobility even in 8ppm DF200. The lack of surface perturbation caused by bubble detachment from the capillary, highlights the effect of frothers on bubble properties even in weakly surface-active frother solution (Figure 5.9a)

The bubbles created in upw achieve the same rising velocity after 50 ms of rising time in both columns. The aspect ratio of the bubbles decreases upon addition of 8 ppm DF200; nevertheless, the change has no effect on the initial rising velocity. In 8 ppm DF250, the adsorbed molecules stabilize the surface immediately turning the bubble to a perfectly spherical shape ($d_h/d_v = 1$). The shape does not change perceptibly during the bubble rising and the decrease of rising velocity becomes apparent within milliseconds (Figure 5.9b).

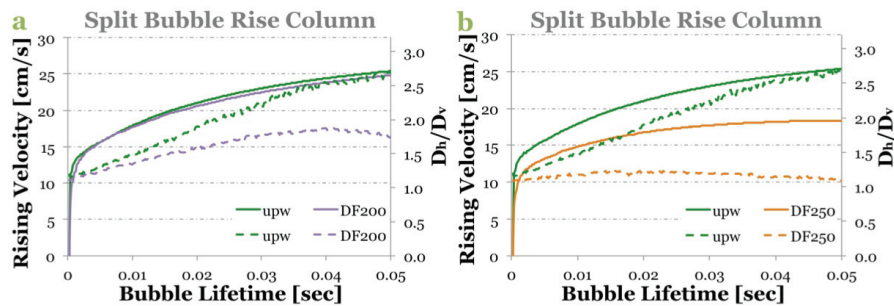


Figure 5.9. Rising velocity (solid line) and aspect ratio (dash line) of the bubble observed in SRVC a) in 8 ppm DF200; b) in 8 ppm of DF250

The results highlight the importance of bubble release technique affecting the rising velocity of the bubbles at low frother concentrations. The difference in surface stabilizing ability between DF200 and DF250 is easily recognisable in presence of surface oscillations. Kracht and Finch (2010) observed similar differences between the 1-Pentanol and PPG425.

5.2.2 Bubble breakup

Walter and Blanch (1986) highlighted the significance of surface stabilizing ability of flotation frothers on bubbles breakup properties.

Figure 5.10 shows the effect of flotation frothers on bubble size distribution in dynamic conditions. The dashed line represents the Sauter mean diameter of the bubbles created in steady-state conditions. In presence of reagent grade surfactants (1-Pentanol and PPG425) the size distribution of the bubbles differs from the one observed in pure water (Figure 5.10a). In 1-Pentanol, the difference is not remarkable; however, the results suggest more frequent bubble breakup. In PPG425, a well recognizable bi-modal size distribution is

obtained, where only small bubbles ($D_{eq} \leq 1$ mm) and bubbles with the created size diameter are present suggesting efficient coalescence prevention ability already at low concentration.

Size distribution results obtained in commercial frother solutions (Figure 5.10b) show some close correspondence between the breakup properties of bubbles in DF200 and that in 1-Pentanol. The similarity is also noticed between DF250 and PPG425.

The bubble size distribution results emphasize smaller minimum D_{eq} in strongly surface-active solutions during bubble breakup than in weakly surface-active solutions. These results do not compromise neither prove the hypothesis of Water and Blanch (1986), which can be due to the relatively small size of created bubbles related to the size of eddies in the turbulent zone. In a particular system condition (constant fluid density, fluid velocity and static surface tension), the increasing bubble size increases the Weber number, and consequently the bubbles become easily unstable (Hinze, 1955).

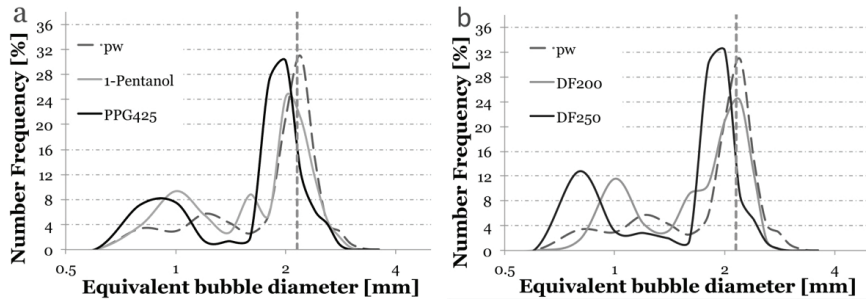


Figure 5.10. The effect of 3 ppm of a) 1-Pentanol and F150 and b) DF200 and DF250 frother solutions on bubble size distribution in dynamic conditions. The bubbles were created with 15 sccm airflow rate

In the present study, the bubble size is controlled with the airflow rate. The high airflow rate (35 sccm) causes coalescence immediately during bubble formation; therefore, the frothers affect bubble size during formation. The frother effect on bubble breakup is examined based on the number frequency of daughter bubbles obtained in dynamic conditions. Although the bubbles that are 90% in volume of the original bubble (mother bubble) can be named as daughter bubbles, in the present work, bubbles are considered daughter bubbles when the diameter is less than half the diameter of the bubbles formed under steady-state conditions. As a consequence, the daughter bubbles in this work are ca. 12% in volume of the mother bubbles. This approach allows studying the formation of small bubbles, with the size similar to the one observed in mechanical flotation cell around the CCC, during bubble breakup. The fraction of daughter bubbles is quantified for every condition. The dashed line in Figure 5.11a represents the size limit of daughter bubbles.

Figure 5.11b presents the number frequency of daughter bubbles created with 35 sccm airflow rate as a function of frother concentration in dynamic conditions. The number frequency of daughter bubbles does not change significantly upon addition of 1-Pentanol; nevertheless the PPG425 reduces the number frequency of daughter bubbles from ca. 23% to ca. 14%.

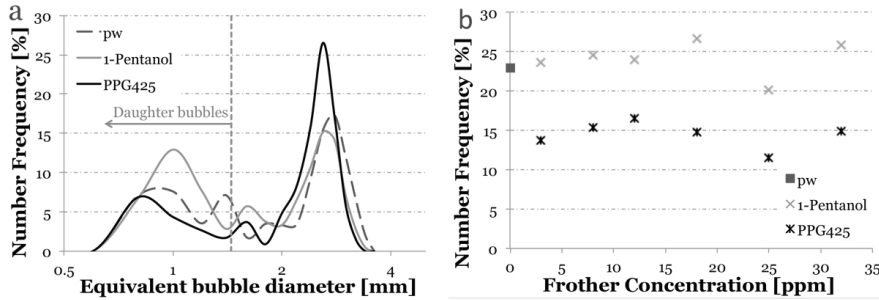


Figure 5.11. a) The effect of 3 ppm of I-Pentanol and F150 frother solutions on bubble size distribution in dynamic condition. The bubbles are created with 35 sccm. b) The effect of increasing frother concentration on the number frequency of daughter bubbles

The breakup results as a function of frother type correspond to the findings of Walter and Blanch (1986). Nevertheless, the increasing frother concentration do not cause noticeable change in the frequency of bubble breakup. The constant and relatively low impeller speed can be the explanation on the phenomenon. The increasing frother concentration should cause more surface perturbation leading to higher population of daughter bubbles; however, the frother is not the only factor that determines surface perturbation (Finch et al., 2008). A high turbulent level is also required to overcome the surface stabilizing ability of frothers.

Highly surface-active frother shows stronger bubble stabilizing ability compared to weakly surface-active ones, but if bubble breakup takes place, a well recognizable bi-modal size distribution is observed in highly surface-active frother solution suggesting efficient coalescence prevention ability already in low concentrations.

5.2.3 Bubble coalescence

Coalescence property of bubbles is investigated in static and in dynamic conditions. In static conditions, when the bubbles are created with one capillary, the effect of frother type and concentration on the size of rising bubbles (D_r) is negligible; however, when the bubbles are created with three capillaries, the importance of frother type and concentration on bubble size becomes apparent (Figure 5.12a).

The size of rising bubbles decreases with increasing frother concentration and becomes uniform upon a particular concentration. The ratio of rising and forming bubbles (D_r/D_f) indicates decrease in bubble size caused by a reduction in number frequency of coalescence (Figure 5.12b). Cho and Laskowski (2002a, b) named the concentration, where the bubbles size becomes uniform, as critical coalescence concentration (CCC).

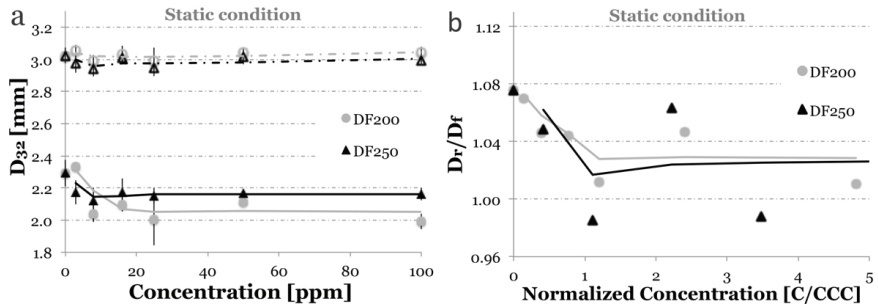


Figure 5.12. a) Frother effect on the size of rising bubble created in static condition with one capillary (dash line) and with three capillaries (solid line). b) Ratio of rising (D_r) and forming bubbles (D_f) as a function of normalized frother concentration in static condition.

The CCC observed in static conditions corresponds to the one measured in mechanical flotation cell. These concentrations are ca. 8 ppm in DF250 and ca. 21 ppm in DF200. The results confirm the theory of Cho and Laskowski (2002a, b), i.e. the size of the bubbles observed in flotation cell are determined by coalescence. However, the bubbles used for studying frother effect on bubble size in mechanical flotation cell are captured from the quiescent zone in order to obtain a reproducible D_{32} results. In laminar conditions, the bubble coalescence is most likely the factor determining the bubble size, nevertheless, in mechanical flotation cell the actual particle-bubble interactions take place in dynamic conditions, where the coalescence can be different from the one observed in the quiescent zone. The validity of CCC theory in dynamic condition was therefore investigated.

The size of the forming and rising bubbles observed in dynamic conditions is shown in Figure 5.13. The D_{32} -C isotherms are normalised with respect to the CCC value for each frother observed in flotation cell. The frother effect on coalescence in dynamic conditions differs from the one obtained in static conditions. It is apparent from the results, in case of DF200, the bubble coalescence is not influenced considerably by the dynamic conditions of the media. On the other hand the results obtained in DF250 suggest that the critical concentration, where the minimum bubble size is reached, is much higher in dynamic conditions than in static condition. The results also reveals that the frother type affect on bubble size already during bubble formation.

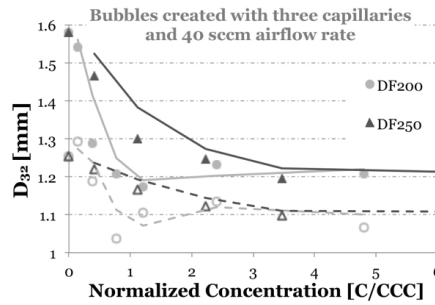
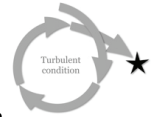


Figure 5.13. Effect of normalized frother concentration on forming (dash line) and rising bubbles (solid line) in dynamic conditions

5.3 Macro-scale results



The effect of flotation frothers on the Sauter mean diameter obtained in mechanical flotation cell is shown in Figure 5.14a. The bubble size decreases with increasing frother concentration from the initial ca. 3.5 mm observed in water and reaches the minimum ca. 0.5 mm diameter in each frother solution.

The highly surface-active PPG425 or DF250 diminishes bubble size significantly already at small concentration and the bubbles reach their minimum size in lower concentration than in weakly surface-active 1-Pentanol or DF200. Table 5.1 summarizes the CCC95 results calculated for each frothers based on the D_{32} -C isotherms. As it is expected based on the D_{32} -C isotherms the CCC95 obtained in 1-Pentanol and DF200 are very close matches as well as the PPG425 with the DF250.

Table 5.2. CCC95 measured at Aalto University²

Flotation frothers	CCC95 [ppm]
1-Pentanol	21.3
DF200	20.8
NF240	15.4
DF250	7.2
PPG425	6.6

The size distribution of the bubbles at equal D_{32} also highlighted sharp differences between the highly surface-active and the weakly surface-active surfactants (Figure 5.14b). Despite the identical D_{32} 's the composition of bubble swarms differs in different frother-solutions. If the reduction in bubble coalescence were the only determining factor in the decrease of D_{32} then the

² The CCC95 data in **Publication II** differs because they were measured at McGill University. A more detailed discussion is found in **Publication V**.

size distribution of the bubbles at equivalent D_{32} , below the CCC, would be identical. The results suggest that the frother type affects not only the magnitude of bubble size decrease but also the swarm composition of the bubbles. The difference in the swarm composition can have a further effect on the efficiency of the flotation process.

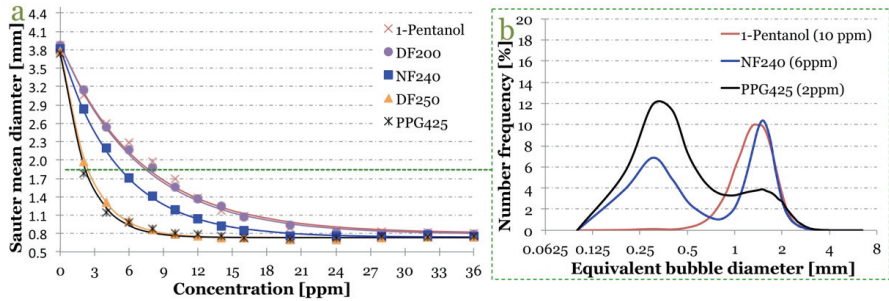


Figure 5.14. a) Concentration effect of flotation frothers on D_{32} . b) Size distribution of the bubbles³ at equal D_{32} ($D_{32} = 1.7$ mm)

The difference of bubble size distribution at equal D_{32} indicates the importance of investigating the phenomenon in more detail. The size distribution of bubbles observed in water highlights two bubble populations (Figure 5.15), i.e. a group of small bubbles with the average diameter of ca. 0.3 (D_{\min}) mm and a group of big bubbles with the average diameter of ca. 3.3 mm (D_{\max}). Nasset et al., (2007) reported similar bi-modal distribution in water.

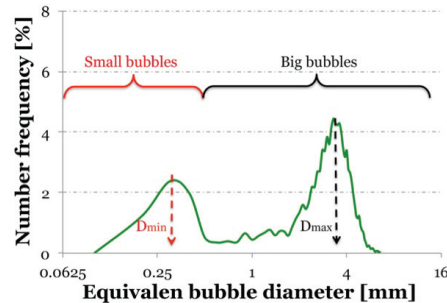


Figure 5.15. The bi-modal bubble size distribution in water where the average diameters of the two bubble populations are marked

In presence of DF200 or 1-Pentanol, the small bubble population disappears (the distribution becomes uni-modal) already upon addition of low concentration of frother and concurrently the D_{\max} decreases. With increasing

³ Note that the x scales of the size distribution figures are logarithmic, here and later on; therefore, the area below the distribution curves cannot be compared directly.

frother concentration the D_{\max} gets smaller and the size distribution curve becomes narrower due to the lower standard deviation (Figure 5.16).

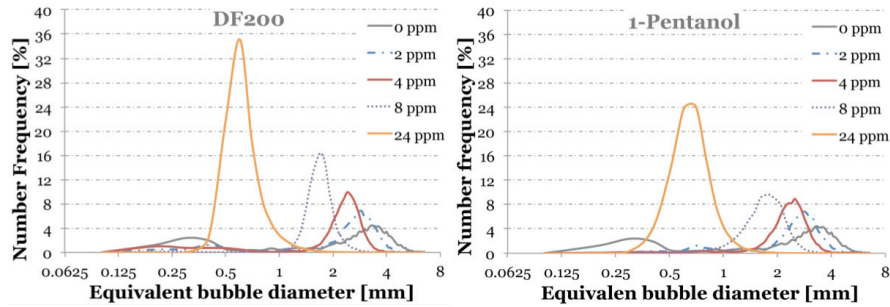


Figure 5.16. Bubble size distribution with increasing frother concentration in DF200 and in I-Pentanol frother solutions

On the contrary, in the presence of DF250 and PPG425, the frother effect on bubble size distribution corresponds well with that described by Nasset et al., (2007), i.e. addition of low concentration of flotation frothers (below the CCC) enhance the bi-modal bubble size distribution observed in water and with increasing frother concentration the size distribution becomes uni-modal (Figure 5.17). The uni-modal distribution is reached around the CCC where the minimum bubble size was also reached.

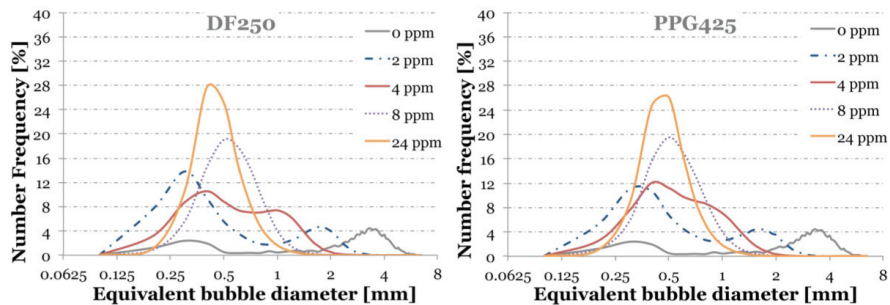
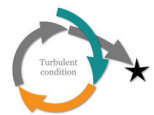


Figure 5.17. Bubble size distribution with increasing frother concentration in DF250 and in F150 frother solutions

5.4 Interactions between scale dependent dynamic properties



There is a close correspondence between the 1-Pentanol and DF200 and also between the PPG425 and DF250 in all the above introduced size-scale studies. Nevertheless, the difference between the two groups is also outstanding in each scale study. In order to quantify the dynamic surface properties leading to particular D_{32} independently on the surface-activity of frothers the dynamic surface properties are investigated at equivalent D_{32} .

The dynamic surface properties obtained at equivalent D_{32} are shown in Figure 5.18. Three frother solutions were studied, e.g. the 10 ppm 1-Pentanol, the 6 ppm NF240 and the 2 ppm PPG425. In all these three frother solutions, the D_{32} observed in mechanical flotation cell is 1.7 mm (Figure 5.14); however, during the dynamic surface property study only the initial dynamic surface tension results ($T_b < 10$ sec) show similarity between the three solutions. These results are in a good agreement with the findings of Comley et al. (2002).

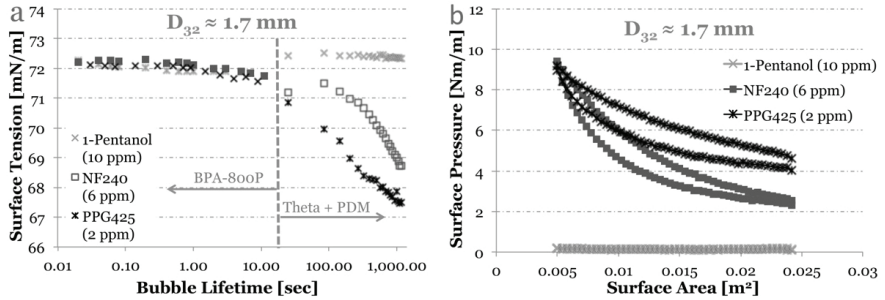


Figure 5.18. The DSP results: a) surface tension vs. time and b) adsorption-desorption hysteresis, measured in individual frother solutions at concentrations where equivalent D_{32} was ca. 1.7 mm ⁴

Beverung et al., (1999) showed that the surface tension does not diminish appreciably in the initial stage of bubble lifetime; therefore, the similar trend in dynamic surface tension in early bubble lifetime cannot be considered as the determining factor on D_{32} without further investigation.

The dynamic properties of the air/liquid interface are identical in 16 ppm NF240 and 3 ppm DF250 solutions (Figure 5.19). In spite of the quantitatively identical DSP, the D_{32} measured in the quiescent zone of the mechanical flotation cell differs. The 16 ppm NF240 is already around the CCC where the D_{32} is ca. 0.85 mm and the size distribution is uni-modal. The 3 ppm DF250 is still way below the CCC where the D_{32} is ca. 1.6 mm and the size distribution is bi-modal. The results highlight that identical DSP's do not even cause similarity in the size distribution model.

Two interesting facts can be concluded based on the findings: the equivalent D_{32} observed in mechanical flotation cell does not imply identical DSP and in case of identical DSP the size distribution curves suggest different coalescence and/or breakup properties. Therefore, if coalescence is considered as the determining factor on bubble size (Cho and Laskowski, 2002) then the findings indicate that the surface elasticity does not play such a crucial role in controlling the bubble size as it was presumed by Grau and Laskowski (2006). But, if the difference in bubble size distribution is caused by the distinction of

⁴ Note that in case of I-Pentanol the surface elasticity is below the measurement threshold of the instrument therefore the elasticity results are not compared.

surface stabilizing ability of surfactants, as it was highlighted by Walter and Blanch (1986), then the results suggest that the type of adsorbed molecules already determines bubble size during formation and breakup.

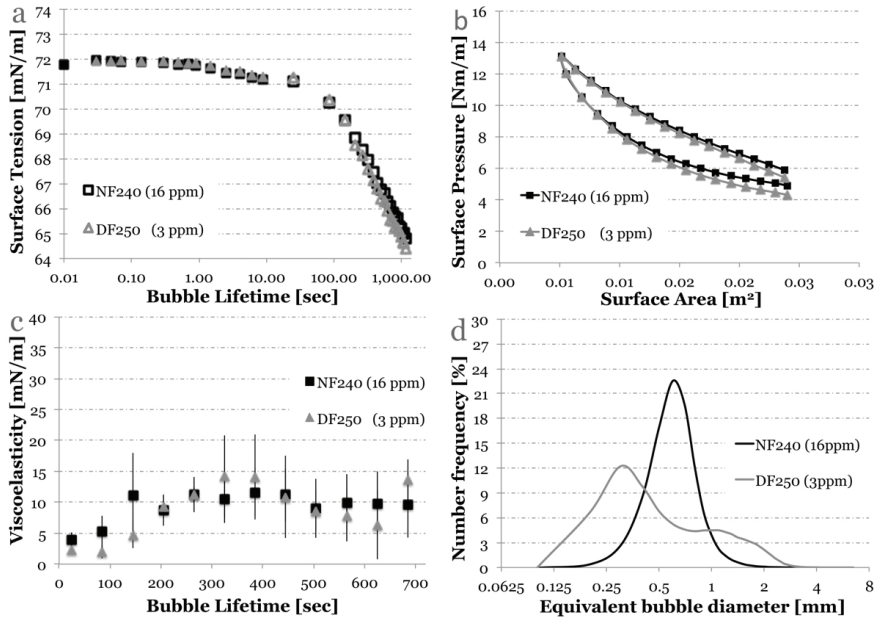


Figure 5.19. a-c) equivalent DSP results observed in individual frother solution and d) the corresponding bubble size distribution curves obtained in mechanical flotation cell

6. Conclusions

A detailed, scale-dependent approach was developed to characterize the effect of frothers on bubble size in dynamic conditions. The change in dynamic properties of the air/liquid interface as the results of the addition of surface-active molecules was studied in three size-scales: micro/nano-, meso- and macro-. Two reagent grade surface active agents (1-Pentanol and PPG425) with distinct properties were employed to characterise the major differences between the two main commercially used frother classes, e.g. alcohols and polyglycols. The results highlight sharp differences between the two frother-types in each size-scale. The key differences are introduced below with regard to the size-scales.

Main conclusions drawn form micro/nano-scale results:

- The surface tension results obtained in 1-Pentanol do not indicate noticeable time and concentration dependency, which would suggest a rapid and only diffusion controlled adsorption; on the contrary, the PPG425 has a significant effect on surface tension and its magnitude is determined by the frother concentration and provided adsorption time suggesting diffusion controlled molecule re-arrangement.
- The surface pressure as a function of surface area variation does not change significantly in 1-Pentanol due to the rapid adsorption/desorption rate of the molecules. On the other hand, in PPG425, the surface pressure fluctuates appreciably as a result of surface area variation. The slow adsorption/desorption rate leads to a hysteresis between the compression and relaxation part of Π -A isotherms as a result of molecule desorption and re-orientation.
- Dilatation surface elasticity arising against hydrodynamic stresses is not detectable in 1-Pentanol; nevertheless, the molecules with slow adsorption/desorption (PPG425) rate lead to a large increase in the surface elasticity.

Main conclusions drawn form meso-scale results:

- The bubble rising velocity results highlight the importance of bubble release technique influencing the surface oscillation of bubbles, and consequently affecting bubble shape. This finding corresponds to the results of Maldonado et al., (2013). The resistance to surface oscillation is higher in PPG425 than in 1-Pentanol.
- The findings also emphasize that the stagnant cap model is not adequate because it disregards the transient phenomena observed on bubble surface as a result of surface oscillations.
- The bubble breakup results confirm the hypothesis of Walter and Blanch (1986); nevertheless, the average diameter of the small bubble population is smaller in PPG425 leading to a well recognizable bi-modal size distribution while in 1-Pentanol the small bubble population is similar to that observed in pure water.
- The bubble coalescence results confirm the hypothesis of Cho and Laskowski (2002a, b); however, the findings also imply that the CCC concept is only applicable in static conditions.

Main conclusions drawn from macro-scale results:

- The PPG425 diminishes bubble size significantly already at low concentration and the bubbles reach their minimum size (ca. 0.5 mm) at lower concentration compared to 1-Pentanol.
- The bi-modal bubble size distribution obtained in water turns to be uni-modal upon addition of small amount of 1-Pentanol, while the addition of PPG425 emphasises the bi-modal distribution and becomes uni-modal when the minimum D_{32} is reached.

The above-introduced findings indicate that the addition of weakly surface-active alcohols cause different changes in the properties of the air/liquid interface compared to the strongly surface-active polyglycols, leading to differences in size-scale properties and eventually in bubble size. These size-scale differences between the 1-Pentanol and PPG425 are shortly summarised in Table 6.1.

Commercial frothers, e.g. DF200 and DF250, were also investigated in detail. From the industrial point of view, the DF200 is a “weak frother” similarly to alcohols while the DF250 is considered as a “strong frother” such as F150 (the commercial name of PPG425). The difference in chemical structure between the two DFs is not that outstanding (only one propylene group) as in case of alcohols and polyglycols; nevertheless, their distinct effect on scale dependent dynamic surface properties and bubble size is also conspicuous (Table 6.2). The impurities contained in commercial frothers might be a possible explanation for the distinct effect of these frothers.

Table 6.1. A summary of the effect of reagent grades surface active agents on scale-dependent surface properties

		1-Pentanol	PPG425
			
Micro/nano-scale	Adsorption/desorption properties	<i>Ineffective</i> in decreasing <i>surface tension</i> (weakly surface active)	<i>Effective</i> in decreasing <i>surface tension</i> (strongly surface active)
	Air/liquid interface properties	During surface perturbation, there is <i>no perceptible elastic property</i>	Surface <i>elasticity arises significantly</i> during surface perturbation and increases with time
Meso-scale	Bubble properties	<i>Bubble surface remains mobile</i> , therefore the breakup and bubble rise behaviour is similar to that observed in pure water	<i>Bubble surface becomes stiff</i> , consequently the rising velocity decreases and surface stability against hydrodynamic stresses increases. However, in case of bubble breakup, the number frequency of small bubbles increases.
	Interaction properties of bubbles	-	-
Macro-scale	Bubble size distribution	<i>Size distribution becomes uni-modal</i> upon addition of small amount of frother	Enhance the bi-modal size distribution observed in water and <i>remains bi-modal until the minimum bubble size</i> is reached
	Sauter mean diameter	<i>The decrease of D_{32}</i> as a function of frother concentration is <i>slow</i>	<i>The decrease of D_{32}</i> as a function of frother concentration is <i>rapid</i>

Table 6.2. A summary of the effect of commercial frothers on scale-dependent surface properties

		DF200	DF250
			
Micro/nano-scale	Adsorption/desorption properties	Weakly surface active <i>Rapid</i> diffusion controlled adsorption and desorption rate	Strongly surface active <i>Slow adsorption</i> and desorption rate suggesting molecule re-arrangement
	Air/liquid interface properties	During surface perturbation, there is <i>no perceptible elastic property</i>	Surface <i>elasticity arises significantly</i> during surface perturbation and increases with time
Meso-scale	Bubble properties	<i>Bubble surface remains mobile</i> , therefore the breakup and bubble rise property is similar to that observed in pure water	<i>Bubble surface becomes stiff</i> , consequently the rising velocity decreases and surface stability against hydrodynamic stresses increases. However, in case of bubble breakup, the number frequency of small bubbles increases.
	Interaction properties of bubbles	The <i>CCC observed in dynamic</i> condition is similar to the one in static conditions	The <i>CCC observed in dynamic</i> condition is much <i>higher</i> than in static conditions
Macro-scale	Bubble size distribution	<i>Size distribution becomes uni-modal</i> upon addition of small amount of frother	Enhance the bi-modal size distribution observed in water and <i>remains bi-modal</i> until the minimum bubble size is reached
	Sauter mean diameter	<i>The decrease of D_{32}</i> as a function of frother concentration is <i>slow</i>	<i>The decrease of D_{32}</i> as a function of frother concentration is <i>rapid</i>

The effect of DF200 on the properties of the air/liquid interface is similar to that of 1-Pentanol in all the three studied size-scales while the effect of DF250 corresponds to that of PPG425. The similarity refers to the tendency and not to the quantity of the results. The close similarity between the DF200 and 1-Pentanol and between the DF250 and PPG425 is easily noticeable; nevertheless, there is no quantitatively determined surface property factor making connection between the two well-distinguished groups. As a consequence, the study of one particular size-scale phenomena alone does not lead to a comprehensive knowledge of frother effect on air/liquid interface.

The physico-chemical picture of the effect of frothers on the air/liquid interface drawn based on the quasi-equilibrium phenomena changes in the presence of local random momentums caused by turbulent eddies. Not all the phenomena taking place in turbulent zone during particle-bubble interactions are predictable with the quasi-equilibrium approach. The present work investigated the dynamic phenomena affecting the bubble size in mechanical flotation cells and brought many insights into the understanding of the frother effect on the properties of the air/liquid interface in turbulent conditions. For example, the type of adsorbed molecules already determines the size of the bubbles during formation and breakup, while the surface elasticity does not play such a crucial role in controlling the coalescence properties of bubbles as it was presumed by Grau and Laskowski (2006). This work makes a further step towards the understanding of the dynamic phenomena taking place in froth flotation.

7. Recommendations for further investigations

The new frother characterization framework introduced in the present work provides a detailed picture of the effect of flotation frothers on the air/liquid interface in turbulent condition and highlights the relationship between the size-scale determined surface properties. Nevertheless, in order to fully understand the phenomena leading to the decrease of bubble size, further size-scale studies are required using the new frother characterization framework. This chapter presents recommendations for further investigations that could advance our knowledge of the effect of flotation frothers on air bubbles in mechanical flotation cell.

The micro/nano-scale measurements show that the adsorption/desorption rate of flotation frothers affecting the dynamic air/liquid interface properties is different for “weak frothers” and “strong frothers”. However, without further investigations this distinct adsorption rate can not be fully explained especially in case of commercial flotation frothers. Therefore studying the orientation of the individual molecules and their effect on the interaction properties of the molecules could help us to understand the phenomena. Such study would also help to characterise the length scale for molecule diffusion and actual adsorption/desorption. Zhang et al (2012) introduced an interesting relationship between D_{32} and the number of carbon atoms in the alkyl group and the position of the functional group. Using a wider range of flotation frothers during the DSP studies could help to explore the connection between DSP and the number of C-atoms.

As it can be concluded based on the meso-scale results the frother type has a significant effect on the breakup properties of air bubbles. The bubble stabilizing ability of air bubbles can be further investigated by using the McGill cell but with different impeller speeds. Characterizing the turbulence created with certain impeller speeds can help to select the proper setting of the experimental set-up in order to fully understand the bubble breakup mechanism governed by turbulence.

The studies also highlighted the importance of shear force on the coalescence of air bubbles. Therefore, the dynamic coalescence as a function of frother concentration should be investigated further in order to define the connection between the frother concentration and the approaching speed of bubbles. The SOC with different circulation speeds of the liquid media and with a wider range of frother types could be used during the study; however some minor changes would be required in order to make even the high concentration measurement more accurate.

In mechanical flotation cell the macro-scale bubble size distribution results showed that in the presence of “strong frothers” more small bubbles are present below the CCC than in “weak frothers”. The comparison of D_{32} -C isotherms and size distribution results between mechanical flotation cell and flotation column could give an indication about the importance of breakup properties in mechanical flotation cell. A more complex and demanding challenge is to introduce a model describing the mass transfer, breakup and coalescence property in dynamic conditions.

The applicability of the frother characterization framework could also be tested with systems where both frother and different types of salts are present.

8. Bibliography

- Allen, T. (1990). Particle size measurement, 4th edition. *Chapman and Hall, T.J. Press Ltd*, Padstow, Cornwall, UK.
- Aybers, N.M., Tapucu, A. (1969a). The motion of gas bubbles rising through stagnant liquid. *Wärme Stoffübertrag*, 2, 118–128.
- Aybers, N.M., Tapucu, A. (1969b). Studies on the drag and shape of gas bubbles rising through stagnant liquid. *Wärme-Stoffübertrag*, 2, 171–177.
- Azgomi, F., Gomez, C.O., Finch J.A. (2007). Characterizing frothers using gas hold-up. *Canadian Metallurgical Quarterly*, 46, 237-242.
- Beverung, C.J., Radke, C.J., Blanch H.W. (1999). Protein adsorption at the oilwater interface: characterization of adsorption kinetics by dynamic interfacial tension measurements. *Biophysical Chemistry* 81, 59-80.
- Biolin Scientific, Attension Theory Note 2. (2014). Static and dynamic surface tension and their measurement techniques. Retrieved from:
http://www.biolinscientific.com/zafepress.php?url=%2Fpdf%2FAttension%2FTheory%20Notes%2FAT_TN_2_surfacetension.pdf
- Biolin Scientific, KSV NIMA Glossary. (2014). Langmuir film. Retrieved from:
<http://www.biolinscientific.com/application/langmuir-film/>
- Castillo, L.A.D., Ohnishi, S., Horn, R.G. (2011). Inhibition of bubble coalescence: Effect of salt concentration and speed of approach. *Journal of Colloid and Interface Science*, 356, 311-324.
- Chalderbank, P.H. (1958). Physical rate processes in industrial fermentation, Part I: The interfacial area in gas-liquid contacting with mechanical agitation. *Transactions of the Institution of Chemical Engineers*, 36, 443-463.
- Chaudhari, R.V. and Hofmann, H. (1994). Coalescence of gas bubbles in liquids. *Reviews in Chemical Engineering*, 10, 131-190.
- Cheng, P., Li, D., Boruvka, L., Rotenberg, Y., Neumann, A.W. (1990). Automation of axisymmetric drop shape analysis for measurements of interfacial tensions and contact angles. *Colloids and Surfaces*, 43, 151-167.
- Chesters, A.K. (1991). The modelling of coalescence properties in fluid-liquid dispersions: a review of current understanding. *Transactions of the Institution of Chemical Engineers*, 69, 259-270.
- Cho, Y.S., Laskowski, J.S. (2002a). Effect of flotation frothers on bubble size and foam stability. *International Journal of Mineral Processing* 64, 69– 80.
- Cho, Y.S., Laskowski, J.S. (2002b). Bubble coalescence and its effect on dynamic foam stability. *The Canadian Journal of Chemical Engineering* 80, 299– 305.
- Clift, R.C., Grace J.R. and Weber M.E. (1978), Bubbles, Drops and Particles. *Academic Press, Inc.* New York, USA.

- Comley, B.A; Harris, P.J; Bradshaw, D.J; Harris, M.C. (2002). Frother characterisation using dynamic surface tension measurements. *International Journal of Mineral Processing*, 64, 81– 100.
- Cuenot, B., Magnaudet, J. and Spennato, B. (1997). Effect of slightly soluble surfactants on the flow around a spherical bubbles, *Journal of Fluid Mechanics*, 339, 25-53.
- Cytec Industries Inc. (2002). Mining chemicals handbook. *American Cyanamid Company*, New York, pp. 75-78.
- Doss, K.S.G. (1939). Alterung der Oberflächen von Lösungen. IV. *Kolloid-Zeitschrift*, 86, 205-213.
- Derjaguin, B.V., Dukhin, S.S. (1961). Theory of flotation of small and medium-size particles. *Transaction of the Institution of Mining and Metallurgy*, 70, 221-246.
- Dukhin, S.S., Kretzschmar, G., Miller, R. (1995). Dynamic of adsorption at liquid interfaces. *Elsevier*, Amsterdam, The Netherlands.
- Fainerman, V.B., Miller, R. (1998). Studies in Interface Science in Mobius, D. and Miller, R. (Editors). Drops and Bubbles in Interfacial Research. *Elsevier*, Amsterdam, The Netherland.
- Finch, J.A., Dobby G.S. (1990). Column flotation. *Permagon Press*, New York, USA.
- Finch, J.A., Gomez, C.O., Hardie, C., Leichtle, G., Filippone, R. and Leroux, D. (1999). Bubble surface area flux: a parameter to characterise flotation cells. *Proceedings of the 31st Canadian Mineral Processors Conference*, Ottawa, 199-210.
- Finch, J.A., Nasset, J.E., Acuña, C. (2008). Role of frother on bubble production and behaviour in flotation. *Minerals Engineering*, 21, 949-957.
- Fruhner, H., Wantke, K.-D., Lunkenheimer, K. (1999). Relationship between surface dilational properties and foam stability. *Colloids and Surfaces, A: Physicochemical and Engineering Aspects*, 162, 193-202.
- Frumkin, A., Levich, V. (1947). On surfactants and interfacial motion. *Russian Journal of Physical Chemistry A (Zhurnal Fizicheskoi Khimii)* 21, 1183.
- Gibbs, I.W. (1948). The collected works of I. Willard Gibbs, *Yale University Press*, New Haven, Vol. 1, pp. 300-314.
- Girault, H.H.J., Schiffrin, D.J., Smith, B.D.V. (1984). The measurement of interfacial tension of pendant drops using a video image profile digitizer. *Journal of Colloid and Interface Science*, 101, 257-266.
- Gomez, C.O., Finch, J.A. (2002). Gas dispersion measurements in flotation machines. *CIM/ICM Bulletin Technical Papers*, 95, 73-78
- Gorain, B.K., Franzidis, J.P., Manlapig, E.V. (1995) Studies on impeller type, impeller speed and air flow rate in an industrial scale flotation cell. Part I: Effect on bubble size distribution, *Minerals Engineering*, 8, 615-635.
- Grainger-Allen, T.J.N. (1970). Bubble generation in froth flotation machines. *Transaction of the Institution of Mining and Metallurgy*, 79, C15-21.
- Grau, R.A., Heiskanen, K. (2002). Visual technique for measuring bubble size in flotation machines. *Minerals Engineering*, 15, 507-513.
- Grau, R.A; Laskowski, J.S. (2006). "Role of frothers in bubble generation and coalescence in a mechanical flotation cell". *The Canadian Journal of Chemical Engineering*, 84, 170-182.
- Hadamard, J.S. (1911). Mouvement permanent lent d'une sphere liquide et visqueuse dans un liquide visqueux. *CR Academy Science*, 152, 1735.
- Hansen, F.K. and Rodsrud, G. (1991). Surface tension by pendant drop: I. A fast standard instrument using computer image analysis. *Journal of Colloid Interface Science*, 141, 1-9

- Harris, C.C. (1976). Flotation machines. In: Flotation, A.M. Gaudin Memorial Volume; Ed.: Fuerstenau, M.C., *American Institute of Mining, Metallurgical, and Petroleum Engineers, Inc.* New York, USA, Volume 2, pp. 753-815.
- Harris, P.J. (1982). Frothing phenomena and frothers. In: Principle of Flotation; Ed.: King, R.P., *South African Institute of Mining and Metallurgy*, Johannesburg, South Africa, pp. 237-250.
- Henry, C.L., Dalton, C.N., Scruton, L. and Craig, V.S.J. (2007). Ion-specific coalescence of bubbles in mixed electrolyte solutions. *The Journal of Physical Chemistry C*, 111, 1015-1023.
- Hernandez-Aguilar, J.R., Gomez, C.O., Finch J.A. (2002). A technique for the direct measurement of bubble size distributions in industrial flotation cells. In: *Proceeding of the 34th Annual Meeting of the Canadian Mineral Processors*, pp. 389-402.
- Hernandez-Aguilar, J.R., Rao, S.R., Finch, J.A. (2005). Testing the k-Sb relationship at the microscale, *Minerals Engineering*, 18, 591-598.
- Hinze, J. O. (1955). Fundamentals of the Hydrodynamic Mechanism of Splitting in Dispersion Processes. *AIChE Journal*, 1, 289-295.
- Janssen, J.J.M., Boon, A. and Agterof, W.G.M. (1994). Droplet breakup in simple shear flow in the presence of emulsifiers. *Colloid and Surfaces A* 91, 141-148.
- King, R.P. (1972). Flotation research work of the N.I.M. research group and the Department of Chemical Engineering, University of Natal, *Journal of the South African Institute of Mining and Metallurgy* 72, 135-145.
- Kirkpatrick, R.D., Lockett, M.J. (1974). The influence of approach velocity on bubble coalescence. *Chemical Engineering Science*, 29, 2363-2373.
- Kolmogorov, A.N. (1941). The local structure of turbulence in incompressible viscous fluids at very large Reynolds numbers, *Doklady Akademii Nauk SSSR*, 30, 299-303. Reprinted in Proceedings: *Mathematical and Physical Sciences*, 434, 9-13 (1991).
- Kracht, W., Finch J.A. (2010). Effect of frother on initial bubble shape and velocity. *International Journal of Mineral Processing* 94, 115-120.
- Krzan, M., Malysa, K. (2002). Profiles of local velocities of bubbles in n-butanol, n-hexanol and n-nonanol solutions. *Colloids and Surfaces A* 207, 279-291.
- Laskowski, J.A. (1998). Frothers and Frothing. In: Laskowski, J.A. and Woodburn, E.T. (Eds.), *Frothing in Flotation II: Recent advances in coal processing*, vol.2. *CRC Press*, pp 1-49.
- Levich, V.G. (1962). Physicochemical hydrodynamics. *Englewood Cliffs, N.J., Prentice-Hall*.
- Lucassen-Reynders, E. H. (1981). Anionic surfactants: Physical chemistry of surfactant action. *Surfactant Science Series*, M. Dekker, New York.
- Lucassen-Reynders, E. H., Lucassen, J. (1994). Surface dilatational viscosity and energy dissipation. *Colloid and Surfaces A* 85, 211-219.
- Lunkenheimer, K. and Kretzschmar, G. (1975). *Zeitschrift für Physikalische Chemie (Leipzig)*, 256, 593
- Machon, V., Vlcer, J. and Kudrna V. (1977) Gas hold-up in agitated aqueous solutions of strong inorganic salt. *Collection Czechoslovak Chemical Communications*, 43, 593-603.
- Machon, V., Pacek, A.W. and Nienow, A.W. (1997). Bubble sizes in electrolyte and alcohol solutions in a turbulent stirred vessel. *Transactions of the Institution of Chemical Engineers*, 75, 339-348.

- Maldonado, M., Quinn, J.J., Gomez, C.O., Finch, J.A. (2013). An experimental study examining the relationship between bubble shape and rise velocity. *Chemical Engineering Science*, 98, 7-11.
- Malysa, K. (1981). Surface elasticity and frothability of n-octanol and n-octanoic acid solutions. *Colloids and Surfaces*, 3, 329-338.
- Malysa, K. (1992). Wet foams: Formation, properties and mechanism of stability. *Advances in Colloid and Interface Science*, 40, 37-83.
- Malysa, K., Lunkenheimer, K. (2008). Foams under dynamic conditions. *Current Opinion in Colloid & Interface Science*, 13, 150-162.
- Marrucci, G. (1969). A theory of coalescence. *Chemical Engineering Science*, 24, 975-985.
- Michel, J.M. (1984). Some features of water flows with ventilated cavities. *ASME Journal of Fluids Engineering*, 106, 319-326.
- Miller, R., Ferri, J.K., Javadi, A., Kragel, J., Mucic, N., Wustneck, R. (2010). Rheology of interfacial layers. *Colloid and Polymer Science*, 288, 937-950.
- Miller, R., Liggieri, L. (2009). Interfacial rheology. Progress in colloid and interface science, *Brill: Leiden*.
- Millet, F., Nedyalkov, M., Renard, B., Perrin, P., Lafuma, F., Benattar, J.J. (1999). Adsorption of hydrophobically modified poly(acrylic acid) sodium salt at the air/water interface by combined surface tension and X-ray reflectivity measurements. *Langmuir* 15, 2112-2119.
- Milner, S.R. (1907). On surface concentration, and the formation of liquid films. *Philosophical Magazine Series* 6, 13, 96-110.
- Mysels, K. (1990). The maximum bubble pressure method of measuring surface tension, revisited. *Colloid and Surfaces*, 43, 241-262.
- Nesset, J.E., Finch, J.A., Gomez, C.O. (2007). Operating variables affecting bubble size in force-airmechanical flotation machines. In: *Proceeding of the 9th Mill Operators Conference*, Fremantle, Australia, 19-21 March, pp. 55-65.
- Nesset, J.E., Zhang, W., Finch, J.A. (2012). A benchmarking tool for assessing flotation cell performance. In: *Proceedings of 2012-44th Annual Meeting of the Canadian Mineral Processors (CIM)*, Ottawa, Canada, 17-19 January, pp. 183-209.
- Pugh, R.J. (1996). Foaming, foam films, antifoaming and defoaming. *Advances in Colloid and Interface Science*, 64, 67-142.
- Pogorely, A.D. (1962). Limits of the use of the kinetic equation proposed by K F Beloglazov. *Izvestiya VUZ. Tsvetnaya Metallurgiya* 1, 33-40.
- Quinn, J.J., Finch, J.A. (2012). On the origin of bi-modal bubble size distributions in the absence of frother. *Minerals Engineering*, 36-38, 237-241.
- Rao, S.R. (2004). Leja, J. Surface Chemistry of Froth Flotation, 2nd ed., *Kluwer Publication*, New York, USA.
- Rennie, J. and Valentin, F.H.H. (1968). Gas dispersion in agitated tanks. *Chemical Engineering Science*, 23, 663-664.
- Richardson, L. F. (1922). Weather Prediction by Numerical Process, *Cambridge University Press*, London, England.
- Rigby, G.D., Evans, G.M., Jameson, G.J. (1997). Bubble breakup from ventilated cavities in multiphase reactors. *Chemical Engineering Science*, 52, 3677-3683.
- Ross, S. (1945). The Change of Surface Tension with Time. I. Theories of Diffusion to the Surface. *Journal of the American Chemical Society*, 67, 990-994.
- Rybczynski, W. (1911). Über die fortschreitende Bewegung einer flüssigen Kugel in einem zähen Medium, *Bulletin Academy of Science Cracovie A*, 40-46.

- Sam, A. (1995). Single bubble behaviors study in a flotation column. Ph.D. Thesis, McGill University Montreal, Canada.
- Sagert, N; Quinn, M; Cribs, S; Rosinger, E. (1976). "Bubble coalescence in aqueous solutions of n-alcohols". In: Akers, R.R. (Ed.), Foams. *Academic Press*, New York, pp. 147-162.
- Savic, P. (1953). Circulation and distortion of liquid drops falling through a viscous medium. Rep. MT-22. National Research Council of Canada, Division of Mechanical Engineering.
- Schwarz, S. and Alexander, D. (2006). Gas dispersion measurements in industrial flotation cells. *Minerals Engineering*, 19, 554-560.
- State Water Board. (2002). Electrical conductivity/salinity fact sheet. In The Clean Water Team Guidance Compendium for Watershed Monitoring and Assessment State Water Resources Control Board. Retrieved from: http://www.waterboards.ca.gov/water_issues/programs/swamp/docs/cwt/guidance/3130en.pdf
- Sweet, C; van Hoogstraten, J; Harris, M; Laskowski, J.S. (1997). The effect of frothers on bubble size and frothability of aqueous solutions. In: Finch, J. A., Rao, S. R., Holubec, I. (Eds.), Processing of Complex Ores-Proc. *2nd UBC-McGill Int. Symp. Metallurgical Society of CIM*, Montreal, pp. 235-245.
- Tse, K.L., Martin, T., McFarlane, C.M., Nienow, A.W. (2003). Small bubble formation via a coalescence dependent breakup mechanism. *Chemical Engineering Science*, 58, 275-286.
- van den Tempel, M., Lucassen-Reynders, E.H. (1983). Relaxation processes at fluid interfaces. *Advances in Colloid and Interface Science* 18, 281-301.
- Walter, J.F; Blanch, H.W. (1986). Bubble breakup in gas-liquid bioreactors: breakup in turbulent flows. *The Chemical Engineering Journal* 32, B7-B17.
- Ward, A.F.H. and Tordai, L. (1946). Time-dependence of boundary tensions of solutions. *The Journal of Chemical Physics*, 14, 453-461.
- Wierink, G.A. (2012). A computational framework for coupled modelling of three-phase systems with soluble surfactants, Ph.D. Thesis, Aalto University Espoo, Finland.
- Wilhelmy, L. (1863). Über die Abhängigkeit der Capillaritäts-Constanten des Alkols von Substanz und Gestalt des benetzten festen Körpers. *Annalen der Physik und Chemie*, 119, 177-217.
- Wrobel, S.A. (1953). Flotation frothers, their action, composition, properties and structure. Recent development in mineral processing, *IMM symposium*, pp. 431-454.
- Xu, M., Finch, J.A. and Uribe-Sala, A. (1991). Maximum gas and bubble surface rates in flotation columns. *International Journal of Mineral Processing* 32, 233-250.
- Yaminsky, V.V., Ohnishi, S., Vogler, E.A., Horn, R.G. (2010). Stability of Aqueous Films between Bubbles. Part 1. The Effect of Speed on Bubble Coalescence in Purified Water and Simple Electrolyte Solutions. *Langmuir*, 26, 8061-8074.
- Zhang, W. (2009). Water overflow rate and bubble surface area flux in flotation. M.Sc. Thesis, McGill University, Montreal, Canada.
- Zhang, W., Nettet, J.E., Rao, R., Finch, J.A. (2012). Characterizing Frothers through Critical Coalescence Concentration (CCC)₉₅ – Hydrophile - Lipophile Balance (HLB) Relationship. *Minerals* 2, 208-227.

The significance of frothers in controlling flotation efficiency is widely acknowledged. However, the mechanism leading to changes in bubble size and eventually in flotation efficiency is not clearly understood.

The present work introduces a new frother characterization framework developed to gain a deeper understanding of the effect of frothers on bubbles in dynamic systems. The new framework systematically explores the chain reaction triggered by the adsorption of frothers and acting along different size-scales. For the first time, a full-scale analysis was accomplished with the primary aim to identify the relationship between the molecular-scale dynamic surface properties (adsorption/desorption, dilatation elasticity) leading to the changes in dynamic bubble properties (rising and breakup) and bubble-bubble interactions (coalescence) that consequently affect the bubble size.



ISBN 978-952-60-5911-2 (printed)

ISBN 978-952-60-5912-9 (pdf)

ISSN-L 1799-4934

ISSN 1799-4934 (printed)

ISSN 1799-4942 (pdf)

Aalto University
School of Chemical Technology
Department of Materials Science and Engineering
www.aalto.fi

**BUSINESS +
ECONOMY**

**ART +
DESIGN +
ARCHITECTURE**

**SCIENCE +
TECHNOLOGY**

CROSSOVER

**DOCTORAL
DISSERTATIONS**